AGU PUBLICATIONS

Journal of Advances in Modeling Earth Systems

RESEARCH ARTICLE
10.1002/2016MS000804

This article is a companion to *Tan et al.* [2016], doi:10.1002/ 2016MS000655.

**Key Points:**
- LES coupled to a slab ocean highlight the important role a closed surface energy balance plays in obtaining realizable subtropical cloud responses to global warming
- Cumulus and stratocumulus cloud regimes consistently exhibit a positive shortwave feedback to warming, with a magnitude that depends, e.g., on large-scale circulation changes and microphysics
- Stratocumulus clouds break up in sufficiently warm climates, as a result of reduced longwave cooling at the cloud top

**Correspondence to:**
Z. Tan,
tanzh@uchicago.edu

**Citation:**
Tan, Z., T. Schneider, J. Teixeira, and K. G. Pressel (2017), Large-eddy simulation of subtropical cloud-topped boundary layers: 2. Cloud response to climate change, *J. Adv. Model. Earth Syst.*, *9*, 19–38, doi:10.1002/ 2016MS000804.

Received 12 SEP 2016
Accepted 18 NOV 2016
Accepted article online 20 DEC 2016
Published online 20 JAN 2017



# Large-eddy simulation of subtropical cloud-topped boundary layers: 2. Cloud response to climate change

**Zhihong Tan [1,2,3], Tapio Schneider [1,2], João Teixeira[2,4], and Kyle G. Pressel [1,2]**

[1]Department of Earth Sciences, ETH Zürich, Zürich, Switzerland, [2]Department of Environmental Science and Engineering, California Institute of Technology, Pasadena, California, USA, [3]Department of Geophysical Sciences, University of Chicago, Chicago, Illinois, USA, [4]Jet Propulsion Laboratory, Pasadena, California, USA

**Abstract** How subtropical marine boundary layer (MBL) clouds respond to warming is investigated using large-eddy simulations (LES) of a wide range of warmer climates, with $CO_2$ concentrations elevated by factors 2–16. In LES coupled to a slab ocean with interactive sea surface temperatures (SST), the surface latent heat flux (LHF) is constrained by the surface energy balance and only strengthens modestly under warming. Consequently, the MBL in warmer climates is shallower than in corresponding fixed-SST LES, in which LHF strengthens excessively and the MBL typically deepens. The inferred shortwave (SW) cloud feedback with a closed energy balance is weakly positive for cumulus clouds. It is more strongly positive for stratocumulus clouds, with a magnitude that increases with warming. Stratocumulus clouds generally break up above 6 K to 9 K warming, or above a four to eightfold increase in $CO_2$ concentrations. This occurs because the MBL mixing driven by cloud-top longwave (LW) cooling weakens as the LW opacity of the free troposphere increases. The stratocumulus breakup triggers an abrupt and large SST increase and MBL deepening, which cannot occur in fixed-SST experiments. SW cloud radiative effects generally weaken while the lower-tropospheric stability increases under warming—the reverse of their empirical relation in the present climate. The MBL is deeper and stratocumulus persists into warmer climates if large-scale subsidence decreases as the climate warms. The contrasts between experiments with interactive SST and fixed SST highlight the importance of a closed surface energy balance for obtaining realizable responses of MBL clouds to warming.

## 1 Introduction

Uncertainties about how subtropical marine boundary layer (MBL) clouds respond to global warming dominate uncertainties in climate change projections [e.g., *Cess et al.*, 1990, 1996; *Bony and Dufresne*, 2005; *Webb et al.*, 2006; *Dufresne and Bony*, 2008; *Vial et al.*, 2013; *Brient et al.*, 2016; *Brient and Schneider*, 2016]. In principle, large-eddy simulation (LES) has the potential to yield quantitatively accurate predictions of how MBL clouds respond to global warming. For example, LES has been successful in reproducing observed features of MBL clouds in the present climate [*Duynkerke et al.*, 1999; *Siebesma et al.*, 2003; *Stevens et al.*, 2005; *Ackerman et al.*, 2009; *Matheou et al.*, 2011; *van Zanten et al.*, 2011]. Such successes in reproducing MBL clouds in the present climate give hope that LES can also be used to study how MBL clouds respond to climate changes. Indeed, LES has been used to study the response of MBL clouds to various changes in large-scale and boundary conditions, in dynamical regimes including shallow cumulus (Cu) [*Bellon and Stevens*, 2012; *Rieck et al.*, 2012; *Schalkwijk et al.*, 2013], stratocumulus (Sc) [*Gesso et al.*, 2014; *van der Dussen et al.*, 2015], and the transition from Sc to Cu [*Chung et al.*, 2012; *Bretherton and Blossey*, 2014]. Within the CFMIP/GASS Intercomparison of Large-Eddy and Single-Column Models (CGILS) LES intercomparison project [*Zhang et al.*, 2012; *Blossey et al.*, 2013], several modeling groups have studied systematically how Sc, Sc-over-Cu, and Cu regimes respond to an idealized 2-K sea surface temperature (SST) increase accompanied by a commensurate increase of free-tropospheric temperatures and a decrease of large-scale subsidence. The response to individual variations in large-scale and boundary conditions has been studied as well [*Bretherton et al.*, 2013]. Such LES studies have explored how different factors external to clouds (e.g., temperature and large-scale subsidence) affect cloud regimes, and they have shed light on diverse mechanisms controlling cloud cover; however, a quantitative understanding of how MBL clouds respond to global warming has remained elusive, in part because it is unclear how individual factors that affect cloud cover change jointly as the climate warms [*Bretherton*, 2015].

Most LES studies of the MBL cloud response to global warming to date have assumed (a) fixed and prescribed-SST changes; (b) independently prescribed and not necessarily energetically consistent changes in radiative parameters (e.g., $CO_2$ concentration); (c) prescribed upper-tropospheric temperature profiles, usually taken to be the moist adiabats corresponding to the prescribed SST. Under these assumptions, the energy budgets of the atmospheric column and the underlying ocean surface are generally not closed. The atmospheric and oceanic energy transports that are implied by the energetic changes may not be realizable in the actual climate system. For example, prescribing similar increases in SST and free-tropospheric temperatures necessitates that the surface latent heat flux (LHF) increases roughly in accordance with the Clausius-Clapeyron relation, provided the relative humidity near the surface changes little. Such a LHF change generally is not realizable: increasing LHF requires an additional energy source, and, for example, the surface radiative forcing resulting from increasing greenhouse gas concentrations usually does not suffice to lead to an LHF increase in proportion to the Clausius-Clapeyron relation [*Boer*, 1993; *Held and Soden*, 2000; *Schneider et al*., 2010]. Because of the excessive LHF increase, the MBL in the LES may become too convective under warming, reducing cloud cover [*Xu et al*., 2010; *Rieck et al*., 2012]. Additionally, the local climate sensitivity in the subtropics may be different from that in the deep tropics, for example, because the subtropical MBL is more effective in longwave (LW) cooling with the much drier free troposphere aloft [*Pierrehumbert*, 1995], or because shortwave (SW) cloud radiative feedbacks modulate the subtropical climate response. Therefore, it may not be valid to assume that the subtropical MBL will warm as much as the free troposphere under global warming. To increase the likelihood that climate changes simulated with LES are realizable, LES studies should be set up so that at least large-scale energetic constraints are explicitly and interactively satisfied.

In a companion paper [*Tan et al*., 2016], we have presented an energetically consistent forcing framework for LES of subtropical MBL clouds. The LES domain is coupled to a 1 m slab ocean model with prescribed ocean heat uptake (OHU) and interactive SST, so that the surface energy budget is closed—a necessary ingredient for realizable climates. The upper troposphere is relaxed to a representative tropical moist adiabat, and the large-scale subsidence velocity and horizontal advection in the lower troposphere are prescribed. With large-scale forcing comparable to the ERA-Interim July climatology of the Global Energy and Water Cycle Experiment Cloud System Study (GCSS) Pacific Cross-Section Intercomparison [*Teixeira et al*., 2011], the MBL regimes studied in the CGILS framework—Sc (CGILS case S12), Sc-over-Cu (S11), and Cu (S6)—are well simulated and are comparable to the CGILS simulations, in which SST are fixed.

In the present paper, we use the forcing framework of *Tan et al*. [2016] to study how subtropical MBL clouds respond to various idealized climate change scenarios. We run multiple simulations with a range of different $CO_2$ concentrations and corresponding upper tropospheric conditions, while OHU is held fixed. We study the MBL cloud response for different combinations of changes in radiative forcing and large-scale subsidence, in an attempt to more clearly delineate which cloud changes can be realized as the climate warms, and to better constrain the MBL cloud feedback to warming.

The paper is organized as follows: section 2 briefly reviews the energetically consistent LES framework and describes the configuration of the climate change experiments. Sections 3 and 4 describe the Cu and Sc responses to $CO_2$-induced warming, respectively. Results from the energetically consistent experiments are compared to those from more conventional experiments with prescribed SST, and the differences in cloud response are discussed. Section 5 summarizes the conclusions.

## 2. Configuration of Climate Change Experiments

### 2.1. Forcing Framework

We use the Python Cloud Large Eddy Simulation (PyCLES) code described in *Pressel et al*. [2015], which uses specific entropy $s$ and total water-specific humidity $q_t$ as prognostic variables. The formulations of the large-scale forcing and energy balance in our LES experiments are described in detail in *Tan et al*. [2016]. To summarize briefly, the large-scale forcing includes three components: large-scale subsidence, lower-tropospheric horizontal advection, and large-scale relaxation toward prescribed temperature and humidity reference profiles in the free troposphere. The large-scale subsidence velocity $\omega_{ls}$ in pressure coordinates is defined as $\omega_{ls}=D\psi(p)$, where $\psi(p)$ is a case-independent kernel profile with maximum at around 700 hPa (about 3000 m), and $D$ is a case-dependent lower-tropospheric divergence rate; the subsidence warming and drying are computed interactively. Prescribed lower-tropospheric horizontal advective cooling and

drying tendencies are applied below 800 hPa (about 2000 m) and are constant in time. Newtonian relaxation toward a reference temperature profile with fixed relative humidity (RH) represents large-scale effects in the free troposphere. The relaxation coefficient is calculated interactively: it is 1 $d^{-1}$ in the interior of the free troposphere and decreases to zero at the simulated MBL top. The surface is formulated as a slab ocean of 1 m depth with prescribed OHU, and the SST is free to evolve according to the surface energy budget. Microphysical and precipitation tendencies are calculated using the Seifert-Beheng scheme [*Seifert and Beheng*, 2001, 2006; *Stevens and Seifert*, 2008]. To represent radiative transfer, we use the Rapid Radiative Transfer Model for GCM Applications (RRTMG) [*Iacono et al*., 2008] with diurnal-mean insolation representative for July conditions. It would also be interesting to study the cloud response to climate changes with a diurnal cycle in a setting similar to ours, to investigate whether a nonlinear rectification of the response as a result of the diurnal cycle occurs, especially for stratocumulus [e.g., *Caldwell and Bretherton*, 2009].

### 2.2. Large-Scale Forcing Under Climate Change

In the climate change experiments, the large-scale conditions (reference profiles, subsidence velocity, and horizontal advective tendencies) are adjusted for each climate state, in a way that is representative of changes that may occur in the climate system when $CO_2$ concentrations increase while other well-mixed greenhouse gas concentrations remain unchanged.

#### 2.2.1. Reference Profiles

Assuming weak temperature gradients (WTG) in the free troposphere between the deep tropics and the subtropics [*Charney*, 1963; *Sobel et al*., 2001], the subtropical reference temperature profile toward which temperatures relax is a radiative-convective equilibrium (RCE) profile representing the deep tropics: we use an adiabat assuming a surface RH of 80%. The tropical surface temperatures are assumed to increase by 3 K per doubling $CO_2$. This is a measure of the tropical equilibrium climate sensitivity (ECS), which is similar to the median of CMIP5 climate models [*Forster et al*., 2013; *Brient and Schneider*, 2016]. Some recent studies [e.g., *Caballero and Huber*, 2010, 2013] have shown that ECS may increase as the climate warms. But because it is uncertain how ECS depends on the climate state, we do not include a state-dependent ECS. As in *Tan et al*. [2016], the subtropical reference RH is assumed to be uniformly 30% below the tropopause. It is 1% just above the tropopause and decreases from there to 0% at the top of the atmosphere. The subtropical reference profiles of specific entropy $s$ and total water specific humidity $q_t$ needed in PyCLES are computed accordingly.

As an alternative to assuming a fixed ECS for the tropics, the tropical surface temperature change could be inferred from the energy balance if one prescribes how the atmospheric and oceanic energy export out of the tropics changes. However, if that energy export were assumed to be fixed at its present value, the strong positive water-vapor feedback would cause the tropical ECS to increase with $CO_2$, eventually leading to a local runaway greenhouse effect [*Pierrehumbert*, 1995]. In reality, the atmospheric and oceanic energy export out of the tropics depends on thermodynamic conditions and large-scale dynamics. Both of them change with climate in complicated ways [e.g., *Caballero and Langen*, 2005; *O'Gorman and Schneider*, 2008a; *Schneider et al*., 2010; *Levine and Schneider*, 2011; *Caballero and Hanley*, 2012], and they stabilize the atmosphere against a runaway greenhouse effect [*Pierrehumbert*, 1995]. Therefore, we prefer the shortcut of fixing the tropical ECS and correspondingly fixing the subtropical reference profiles.

The energy budget of the deep tropics assuming an ECS of 3 K is summarized in Table 1. The required total energy export out of the tropics necessary to maintain the surface temperature implied by an ECS of 3 K is diagnosed to vary from about 50 $W\,m^{-2}$ for the default $CO_2$ concentration of 355 ppm, to 65 $W\,m^{-2}$ for 16 times the default $CO_2$ concentration. These implied energy exports are only representative for the deep tropics, and they do not enter the LES configuration for the subtropics.

#### 2.2.2. Subsidence and Horizontal Advection

In a first set of climate change simulations (FixSub), the tropical overturning circulation strength and the horizontal temperature gradient are assumed to be unchanged under increased $CO_2$ concentrations. Correspondingly, the subsidence velocity, the horizontal wind profiles, and the horizontal advective cooling are also all unchanged. Consistent with assuming an unchanged horizontal temperature gradient and an unchanged spatial pattern of relative humidity, the horizontal advective drying is assumed to scale with the Clausius-Clapeyron relation and increases by 18% per doubling $CO_2$, corresponding to a 3-K ECS and an increase of advective drying of 6% $K^{-1}$. The shapes of the vertical profiles of the subsidence velocity and

**Table 1.** Equatorial Surface Energy Budget From the Offline Calculation of Climate Sensitivity, Assuming That the ECS for the Surface Air Temperature Is 3 K, the Surface Relative Humidity Is 80%, and the Bulk Transfer Coefficient Is Fixed at $C_D||U||=5\times10^{-3}$ m s$^{-1}$[a]

| CASE | OHU (W m$^{-2}$) | SST (K) | TA (K) | SHF (W m$^{-2}$) | LHF (W m$^{-2}$) | RAD (W m$^{-2}$) | LOSS (W m$^{-2}$) |
|---|---|---|---|---|---|---|---|
| 1.0× | 0 | 301.21 | 297.75 | 20.21 | 117.17 | 137.38 | 48.70 |
| | 50 | 299.57 | 297.75 | 10.63 | 86.34 | 146.97 | 50.17 |
| 4.0× | 0 | 306.47 | 303.75 | 15.49 | 138.53 | 154.01 | 54.24 |
| | 50 | 305.07 | 303.75 | 7.51 | 105.15 | 162.65 | 54.96 |
| 16.0× | 0 | 311.67 | 309.75 | 10.69 | 158.54 | 169.23 | 64.32 |
| | 50 | 310.47 | 309.75 | 4.04 | 122.98 | 177.01 | 64.55 |

[a]Two sets of calculations are performed assuming that OHU is 0 and 50 W m$^{-2}$, respectively. The data fields are as follows: $CO_2$ concentration relative to the default value of 355 ppm (CASE); sea surface temperature (SST); surface air temperature; surface sensible heat flux (SHF); surface latent heat flux (LHF); and net radiative energy gain at the surface (RAD). The total energy loss (LOSS) is computed as the sum of atmospheric fluxes and ocean heat export.

horizontal advective tendencies are unchanged, disregarding the increase in tropopause height expected under warming [*Schneider*, 2007].

A second set of climate change simulations (VarSub) also takes the circulation response to warming into account. Under the assumption that the radiative cooling exactly balances the subsidence warming in the free troposphere [*Sobel and Bretherton*, 2000], the large-scale subsidence velocity could be diagnosed in offline radiative transfer calculations using reference profiles for different climates. Such calculations show that the subsidence velocity should decrease by about 40% per doubling $CO_2$ below $2\times CO_2$, and stay almost constant above $4\times CO_2$. However, the diagnosed subsidence velocity for present $CO_2$ concentrations is much lower than observed because horizontal advective cooling is significant in the lower-free troposphere. Especially at the S11 and S12 locations near coasts, where northerly winds prevail, the horizontal advective cooling is comparable in magnitude to radiative cooling, and the subsidence is much enhanced [*Zhang et al*., 2012]. Therefore, the subsidence velocity cannot be constrained by radiative cooling alone. To circumvent the complexities arising from changes in horizontal advection, we simply prescribe a 14.3% decrease of subsidence velocity per doubling $CO_2$, which is consistent with a 3-K ECS and the 5% K$^{-1}$ decrease prescribed in the CGILS LES study [*Blossey et al*., 2013] because $14.3\%=1-0.95^3$. The horizontal wind and advective tendencies are prescribed to be the same as in the FixSub simulations.

The radiative effect of boundary layer clouds affect the column energy budget and feed back onto large-scale circulations such as the Walker circulation [*Peters and Bretherton*, 2005]. Changes in the meridional temperature gradient under warming also affect the horizontal advective tendencies [*Caballero and Langen*, 2005; *Held and Soden*, 2006; *O'Gorman and Schneider*, 2008a; *Caballero and Hanley*, 2012]. *Tan et al*. [2016] showed that experiments with prescribed OHU and interactive SST are sensitive to perturbations in the horizontal advective tendencies. If horizontal advective tendencies decrease under warming, the MBL will be warmer and deeper. A more consistent formulation of subsidence and horizontal advective tendencies requires a closure theory linking these large-scale effects, which is beyond the scope of this study.

### 2.3. Case Studies

We run climate change simulations with five different $CO_2$ concentrations: 1×, 2×, 4×, 8×, and 16× the default $CO_2$ volume mixing ratio of 355 ppm, both for FixSub and for VarSub experiments for the S6, S11, and S12 cases. Varying $CO_2$ concentrations over such a wide range allows us to clearly identify robust mechanisms governing the cloud response to climate changes, in a similar way in which simulations of wide ranges of climates have helped elucidate robust mechanisms governing, e.g., the hydrologic cycle response, extreme precipitation response, or large-scale dynamics response to climate changes [*Walker and Schneider*, 2006; *Schneider and Walker*, 2006; *O'Gorman and Schneider*, 2008a, 2008b, 2009]. The wide range of climates also allow us to investigate the state-dependence of subtropical low cloud feedback, which may lead to enhanced climate sensitivity at high $CO_2$ concentrations, possibly helping to explain climates in Earth's deeper past [*Caballero and Huber*, 2010, 2013].

We run sets of simulations with prescribed OHU (OHU-FixSub and OHU-VarSub) and with prescribed SST (SST-FixSub and SST-VarSub). In the simulations with prescribed OHU, OHU is set as in *Tan et al*. [2016] to 60 W m$^{-2}$ for S6, to 55 W m$^{-2}$ for S11, and to 40 W m$^{-2}$ for S12. The simulations with prescribed SST use the

same configuration as the simulations with prescribed OHU, but SST is set to increase by 3 K per doubling $CO_2$, so that the implied SST difference between the deep tropics and the subtropics is kept fixed.

The horizontal domain size is $L_x = L_y = 6400$ m with resolution $\Delta x = \Delta y = 75$ m, following *Tan et al*. [2016]. The vertical domain depth is $L_z = 5760$ m (S6) and 2880 m (S11 and S12), with resolution $\Delta z = 40$ m (S6) and 20 m (S11 and S12). Note that the domain in the S6 case is deeper in this study than in *Tan et al*. [2016], which necessitates a rougher vertical resolution. The simulated S6 results are not sensitive to this reduction in resolution. We use Weighted Essentially Non-oscillatory (WENO) advection schemes [*Liu et al*., 1994; *Jiang and Shu*, 1996; *Balsara and Shu*, 2000] based on fifth-order interpolations for both momentum and scalars. Following K. G. Pressel et al. (Numerics and subgrid-scale modeling in large eddy simulations of stratocumulus clouds, submitted to *Journal of Advances in Modeling Earth System*, 2016), we disable explicit subgrid-scale (SGS) dissipation beyond the dissipation implicit in the WENO scheme, except in the lowest 200 m, where the Smagorinsky scheme is enabled.

The simulations with prescribed OHU are run for 40 days (S11 and S12) or 75 days (S6). The S6 and S12 cases are in statistically steady states by the end of simulations, but the S11 cases are still slowly drifting (see section 4). The simulations with prescribed SST equilibrate faster and are run for 40 days for all cases. Our analysis focuses on the last 15 days of the simulations.

## 3. Cumulus (S6 case)

All S6 cases are in statistically steady states during the analysis period. Over the 15 day analysis period, the SST drifts by less than $\pm 0.12$ K in the prescribed-OHU cases, and the 6 h-mean surface energy imbalance varies by less than $\pm 10$ W m$^{-2}$ in the prescribed-SST cases. The inversion height, identifiable by the sharp jump of specific humidity $q_t$ across the top of MBL, is diagnosed as the lowest level where $q_t$ is below 1.2 times the free-tropospheric reference $q_t$ [*Tan et al*., 2016]; it varies by less than $\pm 60$ m (i.e., 1.5 vertical levels) in the statistically steady states of all cases. The steady state conditions are summarized in Table 2.

### 3.1. Phenomenology

If the subsidence velocity is fixed, the cloud responses are very different between prescribed SST (SST-FixSub) and prescribed OHU (OHU-FixSub) cases (Figure 1, top plots). SST-FixSub shows slightly increased inversion height, reduced cloud fractions in the top and middle parts of the Cu-layer (hereafter top and mid-Cu fractions), and decreased total cloud cover (CC) under warming. Turbulence strengthens throughout

**Table 2.** Mean Conditions of the S6 Climate Change Experiments During Days 25–40 for Cases With Prescribed SST (SST-FixSub and SST-VarSub), and During Days 60–75 for Cases With Prescribed OHU (OHU-FixSub and OHU-VarSub)[a]

| EXP | $CO_2$ | SST (K) | IMBAL (W m$^{-2}$) | SHF (W m$^{-2}$) | LHF (W m$^{-2}$) | RAD (W m$^{-2}$) | OHU (W m$^{-2}$) | ZINV (m) | LTS (K) | LWP (g m$^{-2}$) | CC (%) | SWCRE (W m$^{-2}$) | PREC (mm d$^{-1}$) |
|---|---|---|---|---|---|---|---|---|---|---|---|---|---|
| OHU-FixSub | 1x | 299 | 0 | 10 | 144 | −215 | 60 | 2881 | 15 | 36 | 22 | 32 | 1.1 |
| | 2x | 301 | −0 | 9 | 150 | −219 | 60 | 2551 | 17 | 33 | 22 | 32 | 0.9 |
| | 4x | 303 | 0 | 7 | 155 | −222 | 60 | 2379 | 19 | 31 | 24 | 32 | 0.8 |
| | 8x | 304 | −0 | 5 | 159 | −224 | 60 | 2258 | 21 | 28 | 26 | 32 | 0.6 |
| | 16x | 306 | −0 | 3 | 166 | −230 | 60 | 2165 | 23 | 24 | 25 | 29 | 0.4 |
| OHU-VarSub | 2x | 302 | 0 | 9 | 151 | −220 | 60 | 2814 | 16 | 35 | 22 | 32 | 1.2 |
| | 4x | 304 | 0 | 7 | 156 | −224 | 60 | 2869 | 18 | 35 | 22 | 32 | 1.3 |
| | 8x | 306 | −0 | 6 | 163 | −228 | 60 | 3031 | 19 | 35 | 22 | 30 | 1.3 |
| | 16x | 308 | −0 | 4 | 170 | −234 | 60 | 3389 | 20 | 32 | 19 | 27 | 1.3 |
| SST-FixSub | 1x | 299 | 7 | 10 | 137 | −214 | 60 | 2715 | 15 | 34 | 22 | 32 | 1.0 |
| | 2x | 302 | −6 | 9 | 158 | −220 | 60 | 2640 | 16 | 33 | 21 | 30 | 1.0 |
| | 4x | 305 | −24 | 7 | 183 | −226 | 60 | 2675 | 17 | 33 | 20 | 29 | 1.1 |
| | 8x | 308 | −44 | 5 | 211 | −232 | 60 | 2755 | 17 | 32 | 18 | 26 | 1.0 |
| | 16x | 311 | −67 | 3 | 242 | −238 | 60 | 2904 | 18 | 30 | 16 | 23 | 0.9 |
| SST-VarSub | 2x | 302 | −1 | 9 | 152 | −220 | 60 | 2862 | 16 | 36 | 22 | 32 | 1.2 |
| | 4x | 305 | −8 | 7 | 167 | −226 | 60 | 3197 | 17 | 36 | 21 | 30 | 1.3 |
| | 8x | 308 | −14 | 5 | 180 | −231 | 60 | 3802 | 17 | 35 | 19 | 28 | 1.3 |
| | 16x | 311 | −15 | 2 | 189 | −236 | 60 | 4683 | 18 | 33 | 17 | 25 | 1.3 |

[a]The surface energy budget terms include sensible heat flux (SHF), latent heat flux (LHF), net radiative cooling (RAD), OHU, and the surface energy imbalance (IMBAL) diagnosed as the residual. Other terms are: sea surface temperature (SST), inversion height (ZINV, defined as the lowest level where $q_t < 1.2q_{t,\mathrm{ref}}$), lower tropospheric stability (LTS, defined as $\theta_{700\mathrm{hPa,ref}} - \theta_{\mathrm{sfc}}$), liquid water path (LWP), total cloud cover (CC), surface SWCRE, and surface precipitation rate (PREC).

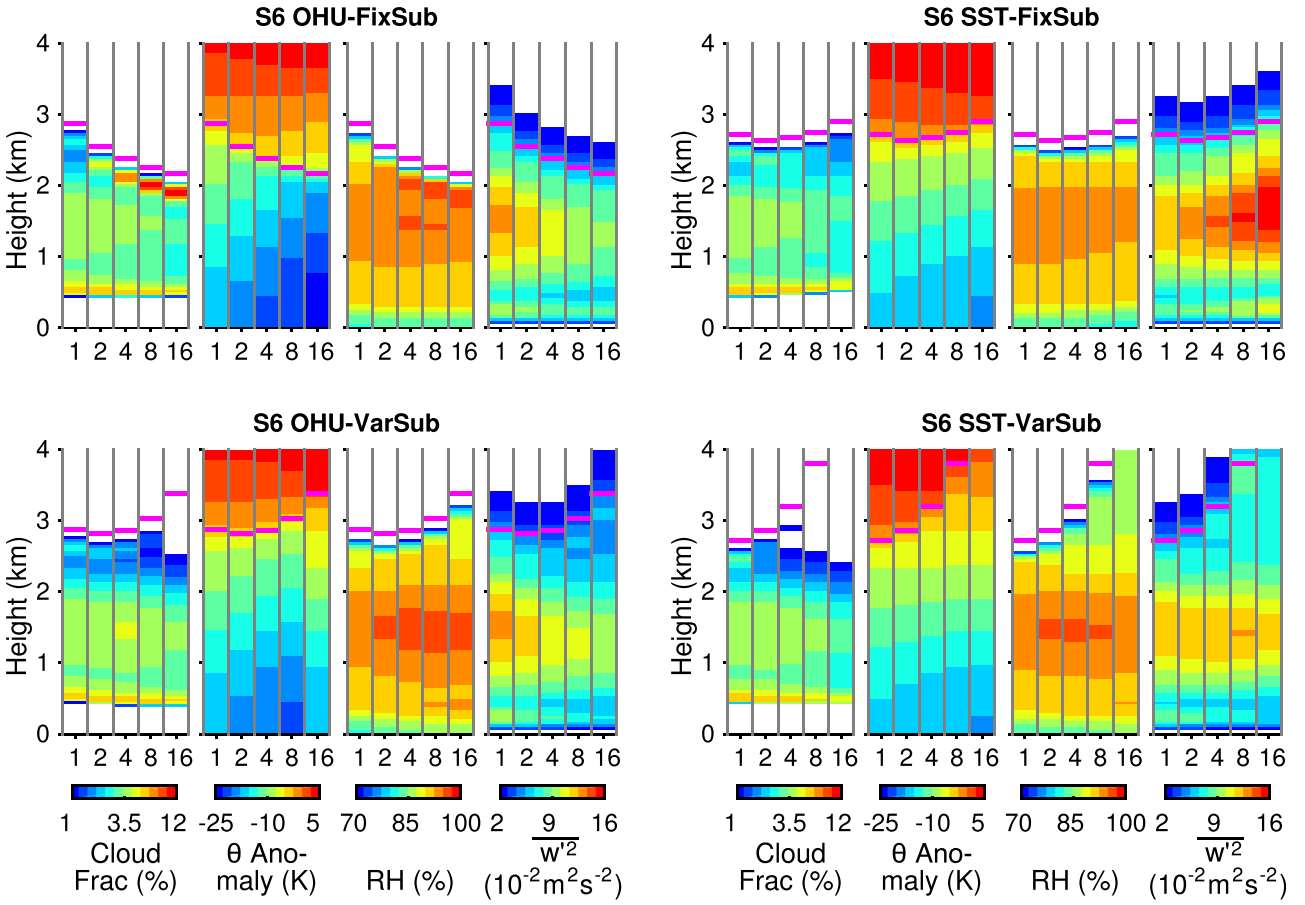


**Figure 1.** Statistical steady state profiles of the S6 climate change experiments: cloud fraction, potential temperature $\theta$ anomaly compared to the reference value at 700 hPa, relative humidity (RH), and resolved variance of vertical velocity. The solid magenta lines represent the inversion heights. The $x$ axis is the ratio between the $CO_2$ concentration in each case and the default value (355 ppm). (top row) Experiments with fixed subsidence. (bottom row) Experiments with weakening subsidence under warming. (left column) Experiments with prescribed OHU and freely adjusting SST. (right column) Experiments with prescribed SST.

the MBL, but surface precipitation is almost unchanged: the increased evaporation is mostly compensated by increased subsidence drying, reflecting the fact that the LES domain is not closed with respect to the water balance. The lifted condensation level (LCL) rises only slightly. In contrast, OHU-FixSub shows significantly reduced inversion height and much larger top-Cu fraction, as well as an increased inversion strength under warming. The total CC is dominated by the top-Cu fraction and increases under warming. Turbulence weakens throughout the MBL, and the surface precipitation weakens substantially too, while the LCL remains unchanged (Table 2).

The contrast between prescribed-SST and prescribed-OHU cases is much reduced if subsidence weakens with warming (Figure 1, bottom plots). Both SST-VarSub and OHU-VarSub show increased inversion height and decreased top-Cu fraction under warming. In the warmest cases, although Cu updrafts occasionally penetrate up to the inversion, the Cu fraction in the upper part of MBL is very small (less than 1%). The mid-Cu fraction increases slightly under modest warming, but it decreases significantly in the warmest cases. OHU-VarSub is cooler and less convective than SST-VarSub, with a smaller increase in inversion height and weaker turbulence relative to SST-VarSub, analogous to the corresponding simulations with fixed subsidence. In both cases with weakening subsidence, surface precipitation increases up to $4\times CO_2$ and levels off under further warming, similar to what is seen in GCM simulations, because the additional energy needed to evaporate water levels off as the atmosphere becomes optically thick for longwave radiation [*O'Gorman and Schneider*, 2008a].

### 3.2. Interpretation Based on Energy Budget

The contrast between OHU-FixSub and SST-FixSub cloud responses can be understood from their surface and MBL energy budgets, as shown in the schematic Figure 2.

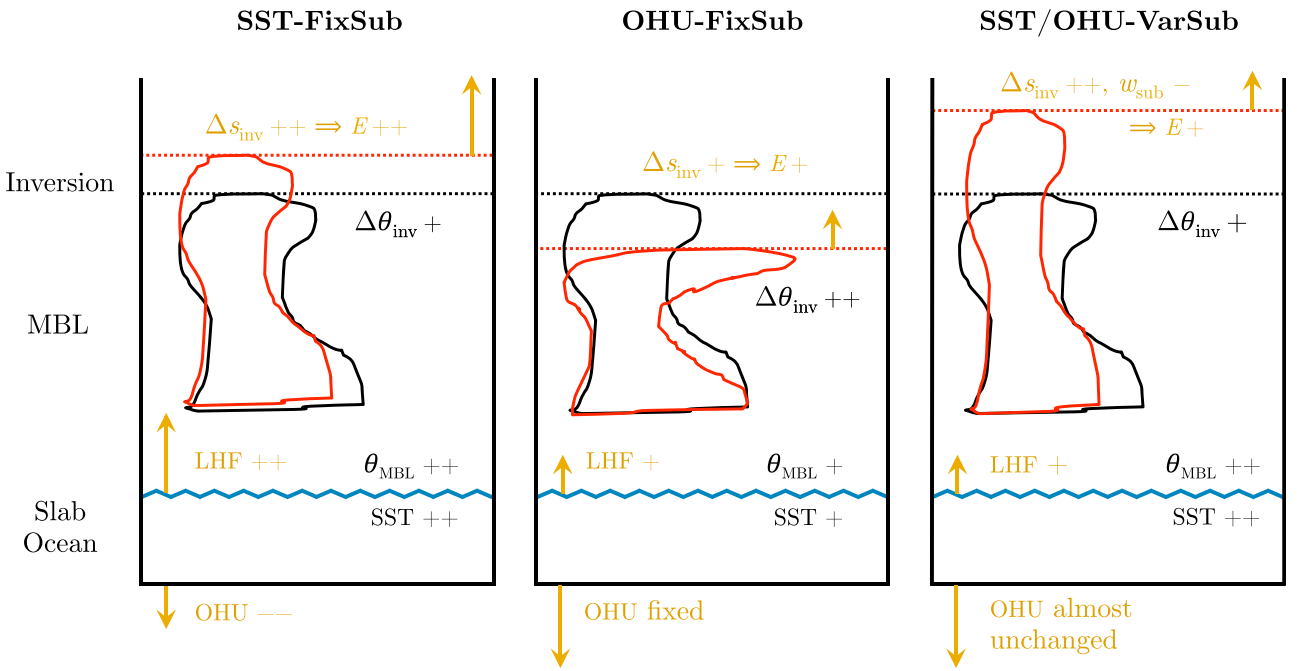


**Figure 2.** Schematic of Cu response under different configurations. The red outlines represent Cu clouds in a warmer climate than the corresponding clouds in black outlines. The dashed lines represent inversion heights in warmer (red) and reference (black) climates, and the blue wavy lines represent the ocean surface. Orange arrows represent the surface and MBL energy sources and sinks. Here, $E$ represents the loss of MBL moist static energy due to entrainment across the inversion, $\Delta\theta_{inv}=\theta_{FT}-\theta_{MBL}$ is the inversion strength, and $\Delta s_{inv}=s_{MBL}-s_{FT}$ is the moist static energy jump across the inversion.

SST-FixSub assumes that SST and thus the MBL temperature increase like the free-tropospheric temperature. The advective and entrainment drying in the MBL both increase according to the Clausius-Clapeyron relation (at approximately 6 % $K^{-1}$), and thus the MBL moisture budget requires that the surface LHF also increases by roughly as much: by 7–10 W $m^{-2}$ $K^{-1}$, or about 5 % $K^{-1}$ (Figure 3). Or, from the perspective of the surface energy budget, relative humidity changes near the surface are small, and evaporation is primarily controlled by the subsaturation of near-surface air, which, at nearly constant relative humidity, increases with the saturation specific humidity as the climate warms; this also gives the result that LHF increases roughly at the Clausius-Clapeyron rate. At the same time, the surface sensible heat flux (SHF) decreases robustly by 0.3–0.9 W $m^{-2}$ $K^{-1}$. The decrease in SHF is consistent with what is seen in climate model simulations and can be understood from the increase in LHF and the decrease in the Bowen ratio (the ratio between SHF and LHF) under warming [*Mitchell et al.*, 1987; *Pierrehumbert*, 2002; *O'Gorman and Schneider*,

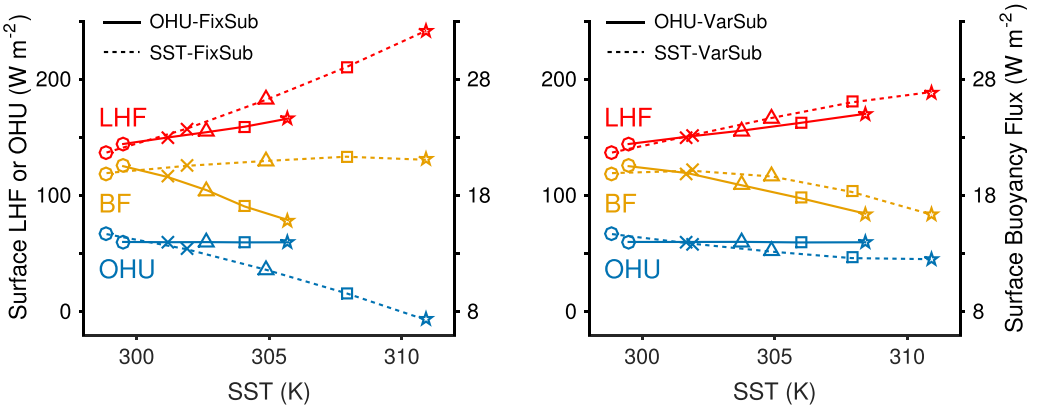


**Figure 3.** Surface LHF (red), required OHU for surface energy balance (blue), and buoyancy flux (orange) for the S6 climate change experiments versus SST. (left) Fixed subsidence. (right) Weakening subsidence under warming. (solid) Prescribed OHU. (dashed) Prescribed SST. (circles) 1x; (crosses) 2x; (triangles) 4x; (squares) 8x; and (pentagrams) 16x $CO_2$ concentration.

2008a; *Lu and Cai*, 2009; *Webb and Lock*, 2013]. The reduced SHF compensates for the increased subsidence warming and reduced radiative cooling in the dry static energy budget of MBL. The surface buoyancy flux (BF) consists of contributions from both SHF and LHF and can be approximated as follows:

$$\mathrm{BF} = \mathrm{SHF} + \left(\frac{R_v}{R_d} - 1\right)\frac{c_p T_s}{L_v}\mathrm{LHF} \approx \mathrm{SHF} + 0.08\,\mathrm{LHF}. \quad (1)$$

Here, $c_p$ is the isobaric heat capacity of air, $R_d$ and $R_v$ are the specific gas constants of dry air and water vapor, $L_v$ is the latent heat of vaporization, and $T_s$ is the surface temperature. In SST-FixSub, the strong increase in LHF dominates over the weak decrease in SHF in their contribution to the BF (1), so that BF increases, especially under modest warming (Figure 3). Increases in both BF and LHF contribute to strengthened turbulence throughout the MBL (see $\overline{w'^2}$ in Figure 1), especially in the mid-Cu layer. This maintains the MBL-top entrainment and slightly increases the inversion height.

However, the surface energy budget of SST-FixSub is not closed. The increased energy loss by LHF cannot be compensated by the relatively weak decrease in SHF and LW radiative cooling, and thus the net surface energy gain (SEG, defined as the SW heating minus the sum of SHF, LHF, and LW cooling) decreases significantly. This requires OHU to decrease by 6 $\mathrm{W\,m^{-2}\,K^{-1}}$ on average to maintain the surface energy balance. The required OHU eventually changes sign when $CO_2$ concentrations exceed about 14 times the default value. Ocean heat release in the subtropics seems unphysical; this is one reason why simulations with prescribed OHU are to be preferred over those with prescribed SST.

In contrast, OHU-FixSub enforces the surface energy balance with fixed OHU. This requires that the surface LHF can only increase as much as the decrease in SHF and LW radiative cooling allows (Figure 3). Therefore, the increase in LHF is much weaker under warming (3–4 $\mathrm{W\,m^{-2}\,K^{-1}}$, or about $2\,\%\,\mathrm{K^{-1}}$), and BF decreases robustly, since the decrease in SHF dominates over the weak increase in LHF in equation (1). Both trends in LHF and BF lead to a shallower and less convective MBL with weaker turbulence under warming. The SST and MBL temperatures only increase by about 1.6 K per doubling of $CO_2$. This can be understood from the MBL energy budget: a hypothetical larger increase in MBL temperature (e.g., 3 K as in SST-FixSub) would imply a too large moist static energy jump at the inversion and too much entrainment energy loss, which cannot be balanced by the weak increase in LHF.

The sensitivity of subtropical MBL clouds to surface fluxes was previously studied by *Webb and Lock* [2013] with a GCM. They also found that a weaker increase in LHF than the Clausius-Clapeyron relation and a robust decrease in SHF led to weakened turbulent mixing in MBL, resulting in reduced SWCRE. However, the Cu responses in our study are not directly comparable to their results with fixed SST, which lacked the SST feedback that causes MBL shallowing and increased inversion strength in our OHU-FixSub cases.

The contrasts between the cases with fixed OHU or fixed SST and with varying subsidence (OHU-VarSub and SST-VarSub) are less pronounced. With reduced subsidence, the entrainment moist static energy loss in SST-VarSub is weaker, primarily because of the direct effect of reduced entrainment rates that balance the reduced subsidence; the reduced RH jump across the inversion also contributes. So the required moist static energy gain by LHF is less (only about $3\,\%\,\mathrm{K^{-1}}$). This brings the LHF fluxes in the SST-VarSub case closer in alignment with the cases with fixed OHU, reducing differences between the cases. The implied OHU in SST-VarSub only needs to decrease slightly (by about 2 $\mathrm{W\,m^{-2}\,K^{-1}}$) to balance the weak increase in LHF. The SST-VarSub surface energy budget is thus much closer to that of OHU-VarSub, and so their steady states are also more similar. SST-VarSub still has a warmer, deeper, and more convective MBL than OHU-VarSub, since its LHF still is larger. Thus, including a reduced subsidence renders the cases with fixed SST closer to being realizable, albeit by a fortuitous compensation between the surface energy balance and subsidence effects.

### 3.3. Implications for Shortwave Cloud Radiative Effects

The liquid water path (LWP), CC, and shortwave cloud radiative effect (SWCRE) in the steady states for all cases are shown in Figure 4. As discussed in *Tan et al.* [2016], the magnitude of SWCRE depends on two factors: the column-integrated LWP and the total CC. LWP is mostly contributed by the mid-Cu layer, and thus it is positively correlated with the Cu-layer depth and the mid-Cu fraction. The mid-Cu fraction generally increases when diabatic cooling is enhanced, including horizontal advection, subsidence, and radiative cooling, since these processes destabilize the Cu layer and activate the Cu updrafts. The mid-Cu fraction

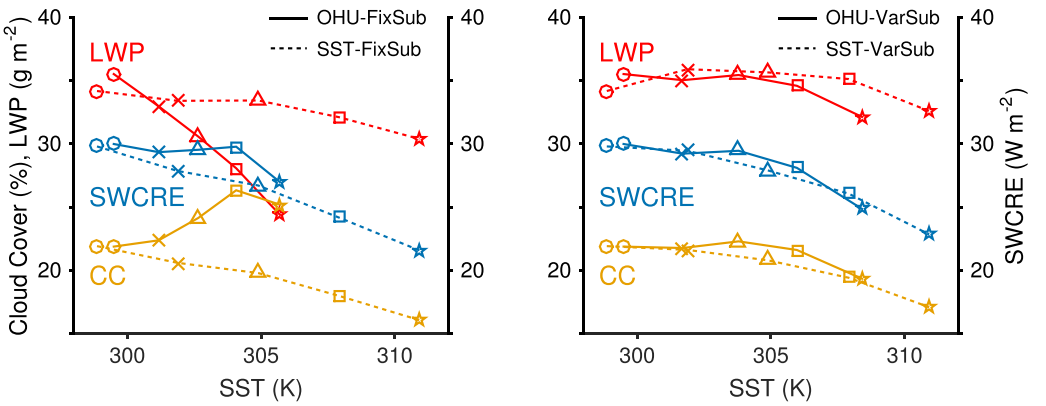


**Figure 4.** Same as Figure 3, but for total cloud cover (orange), LWP (red), and surface SWCRE (blue).

also increases as a result of cooling and moistening associated with rain re-evaporation. CC is more dependent on the top-Cu fraction, which is related to the inversion strength.

For the SST-FixSub cases, the top-Cu fraction is insignificant and the Cu-layer depth does not change much. Therefore, both LWP and CC depend primarily on the mid-Cu fraction, which decreases under warming, and thus the magnitude of SWCRE decreases by about 2.1 W m$^{-2}$ per doubling of $CO_2$ (or by 0.7 W m$^{-2}$ per 1 K local warming).

The mid-Cu fraction is primarily controlled by the updraft fraction $a_u$. The mid-Cu fraction decreases because the updraft fraction $a_u$ decreases, a result of the combined effect of an almost unchanged updraft velocity ($w_u$) and a decreased updraft mass flux ($m_u$), since $a_u = m_u/w_u$. The weak change in $w_u$ under warming can be understood from the arguments made by *Singh and O'Gorman* [2013, 2015]: the updraft velocity $w_u$ of a weakly entraining (i.e., the most buoyant) updraft only increases slightly (by about 1% K$^{-1}$) below 3 km, assuming that the environment is neutrally buoyant with respect to a moderately entraining updraft and that both entrainment rates do not change; the change in $w_u$ of the bulk mean updraft can be expected to scale similarly. The decrease in $m_u$ agrees with the mechanism described by *Betts and Ridgway* [1989] and summarized by *Schneider et al*. [2010]: the latent heating per unit mass flux $m_u$ increases with $dq_s/dp$ (by about 4% K$^{-1}$ for a subtropical MBL), while total latent heating remains in balance with LW cooling, which generally weakens due to increased free tropospheric LW opacity. The decrease in $m_u$ is weaker below 4× the default $CO_2$ concentration, when the free troposphere is optically thin and the MBL moistening leads to a slight increase in LW cooling. Consequently, the decreases in $a_u$ and mid-Cu fraction are less significant under modest warming. Note that the mid-Cu fraction includes contributions from detraining shallower Cu, whose area fraction cannot be constrained by $a_u$ locally (but it is related to $a_u$ at lower levels). The exact relation between $a_u$ and Cu fraction requires further investigation.

For the OHU-FixSub cases, the decrease in LWP is sharper because the Cu layer shallows. The mid-Cu fraction still decreases, but the increased top-Cu fraction under the stronger inversion leads to an increase in total CC. These counteracting effects add up to a reduction in the magnitude of SWCRE, which is only 0.2 W m$^{-2}$ per doubling of $CO_2$, or about 0.14 W m$^{-2}$ per 1 K local warming. However, the top-Cu fraction is sensitive to the choice of microphysics scheme. The SWCRE response is stronger with schemes that have higher precipitation efficiencies and are less favorable for the formation and maintenance of top-Cu (anvils) just below inversion. This illustrates the sensitivity of Cu feedback to precipitation microphysics [*Zhao et al*., 2016], which has proven difficult to constrain observationally or from first principles.

The OHU-VarSub and the SST-VarSub cases are both similar to the SST-FixSub cases. In both cases, the magnitude of SWCRE decreases strongly under warming, since the mid-Cu fraction decreases and the top-Cu fraction is insignificant. The reduction in SWCRE is about 0.6 W m$^{-2}$ per 1 K local warming for both OHU-VarSub and SST-VarSub, but the reduction per doubling of $CO_2$ is slightly weaker for OHU-VarSub since it warms less. The reduction in SWCRE by 0.6 W m$^{-2}$ per 1 K local warming is consistent with the most likely SWCRE inferred by weighting global-warming simulations with comprehensive climate models according to how well they reproduce deseasonalized variations of low-cloud cover [*Brient and Schneider*, 2016].

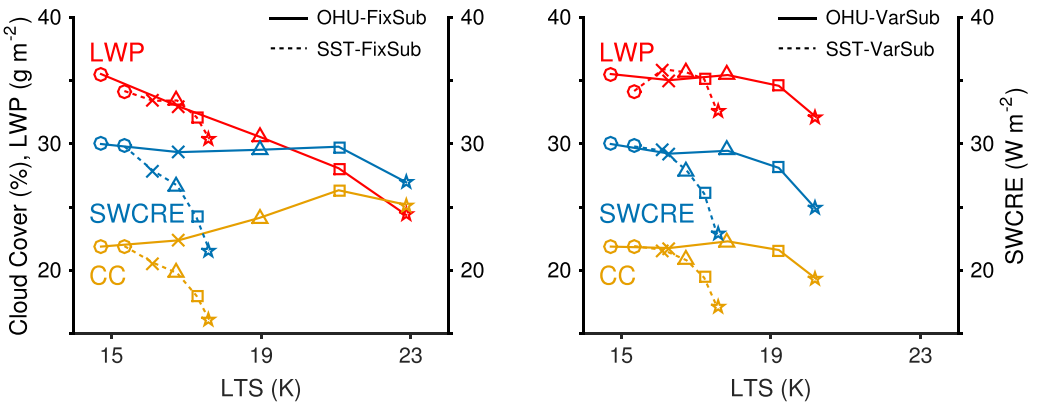


**Figure 5.** Same as Figure 4, but the cloud variables are plotted against LTS.

### 3.4. Relation of SWCRE to Lower-Tropospheric Static Stability

Indicators of the inversion strength, such as the lower-tropospheric static stability (LTS) and variants thereof, have often been invoked as factors controlling low-cloud cover [*Klein and Hartmann*, 1993; *Wood and Bretherton*, 2006]. However, *Medeiros and Nuijens* [2016] showed that LTS may not be a good predictor of variations in the subtropical Cu fraction. Figure 5 shows the LWP, CC, and SWCRE as functions of the LTS, defined as the potential temperature difference between 700 hPa and the surface. In our analysis, the reference potential temperature at 700 hPa is used instead of the in situ potential temperature for all cases. This provides a better indication of inversion strength when the Cu layer grows deeper than 700 hPa (e.g., in the warmest cases of OHU-VarSub and SST-VarSub), where the in situ potential temperature is no longer related to free tropospheric temperature. For cases with shallower Cu layer, this definition gives a similar LTS as the conventional definition with in situ potential temperatures.

Generally, the LTS is larger in our experiments with prescribed OHU, because they have lower SST than the corresponding experiments with prescribed SST, while the free-tropospheric temperatures are similar. Since the SWCRE is also stronger in the prescribed-OHU cases, when comparing prescribed-OHU and prescribed-SST cases at the same $CO_2$ concentration, there appears to be a positive correlation between LTS and SWCRE. This has some semblance to the observed LTS-CC relation presented in *Klein and Hartmann* [1993].

However, this correlation is reversed in the context of climate change, when $CO_2$ concentrations increase. LTS strengthens systematically under warming, while SWCRE weakens in all cases, implying a negative correlation between SWCRE and LTS under climate change (Figure 5). However, there remains a positive correlation between CC and LTS in the OHU-FixSub cases, because of the formation of top-Cu just under the inversion. The reversed SWCRE-LTS relation, and in some cases the reversed CC-LTS relation, agree with *Lauer et al*. [2010], who also found that the simulated LTS and CC under global warming did not follow the present-day empirical relationship. These results emphasize that caution needs to be exercised when empirical relationships in the present climate are used for inferences about changed climates.

### 3.5. Summary

The key results of the Cu (S6) climate change cases can be summarized as follows:

1. Both SST and OHU experiments are sensitive to the prescribed large-scale subsidence. The FixSub cases show a decrease or weak increase in MBL depth under warming, while the VarSub cases show significant MBL deepening.
2. Positive Cu SW feedback is simulated in all cases. The SWCRE decreases by 1.8 to 2.1 $W\,m^{-2}$ per doubling of $CO_2$, or by 0.6 to 0.7 $W\,m^{-2}$ per 1 K warming. This is in line with the most likely SWCRE inferred from comprehensive climate models under global warming [*Brient and Schneider*, 2016]. However, the decrease is much weaker in the OHU-FixSub case because of the increased top-Cu fraction under the strengthened inversion, a result that is sensitive to the formulation of precipitation microphysics [cf. *Zhao et al*., 2016].
3. The SST-FixSub case has a large increase in surface LHF, and the surface energy budget is not closed. This illustrates that experiments with prescribed SST, as in several previous LES studies [e.g., *Xu et al*.,

2010; *Rieck et al.*, 2012], can lead to fundamentally different MBL dynamical balances than are realizable under climate change.

4. The SST-VarSub and OHU-VarSub cases are much more alike in their energy budgets and cloud responses, because of compensation between subsidence and surface energy balance effects. Both show systematic reductions in CC and LWP due to decreased mid-Cu fraction, which is responsible for their robustly positive SW feedbacks.
5. LTS increases while SWCRE weakens as the climate warms. This is opposite to their positive correlation in the current climate.

## 4. Stratocumulus (S11 and S12 Cases)

The S11 and S12 cases with prescribed SST (SST-FixSub and SST-VarSub) generally reach statistically steady states in about 10 days, since their Sc-topped MBL are relatively shallow. However, the equilibration timescale is much longer (15–20 days) for cases in which the Sc layer breaks up. The Sc layer in the S11 SST-VarSub 16×$CO_2$ simulation grows beyond the top of the model domain (2880 m); this simulation is excluded in what follows.

The S11 and S12 cases with prescribed OHU (OHU-FixSub and OHU-VarSub) equilibrate much more slowly with their interactive SST. The S12 (Sc) cases reach steady states around days 25–35, irrespective of whether the Sc layer breaks up or not. The S11 (Sc-over-Cu) cases generally do not reach steady states even after 40 days: the SST decreases by 0.5–1.5 K from day 20 to day 40, during which the MBL shallows continuously and LWP increases. This is a positive SW cloud feedback that may terminate in a well-mixed Sc steady state. The only S11 cases that reach steady states are the OHU-FixSub cases with 8× and 16×$CO_2$, in which the Sc layer breaks up and transitions into a steady Cu regime by day 40.

The mean conditions during days 30–40 are summarized in Tables 3 and 4. Figures 6 and 7 show the average vertical profiles, Figure 8 shows the surface energy budget, and Figure 9 shows the average LWP, CC, and SWCRE. Except for the S11 OHU-VarSub and SST-VarSub cases, all other S11 and S12 experiments show that the Sc layers break up when $CO_2$ concentrations increase above 4× (S12) or 8× (S11) their default value of 355 ppm. This cloud regime transition is robust under both prescribed-SST and prescribed-OHU configurations.

### 4.1. Sc Layer Response Under Modest Warming

At $CO_2$ levels below the transition threshold, all experiments with prescribed SST show a continuous decrease in LWP and weakening of MBL turbulence under warming because cloud-top cooling weakens as the infrared opacity of the overlying free troposphere increases. The diminishing LWP feeds back positively onto the diminished cloud-top cooling. This general tendency is robust for both SST-FixSub and SST-VarSub

**Table 3.** Mean Conditions of the S11 Climate Change Experiments During Days 30–40[a]

| EXP | $CO_2$ | SST (K) | IMBAL (W m$^{-2}$) | SHF (W m$^{-2}$) | LHF (W m$^{-2}$) | RAD (W m$^{-2}$) | OHU (W m$^{-2}$) | ZINV (m) | LTS (K) | LWP (g m$^{-2}$) | CC (%) | SWCRE (W m$^{-2}$) | PREC (mm d$^{-1}$) |
|---|---|---|---|---|---|---|---|---|---|---|---|---|---|
| OHU-FixSub | 1x | 292 | −2 | 2 | 86 | −141 | 55 | 1608 | 22 | 53 | 100 | 158 | 0.0 |
| | 2x | 293 | −4 | 1 | 86 | −139 | 55 | 1376 | 24 | 57 | 100 | 161 | 0.0 |
| | 4x | 296 | −3 | 1 | 101 | −154 | 55 | 1328 | 25 | 47 | 99 | 142 | 0.0 |
| | 8x | 303 | 0 | 3 | 173 | −231 | 55 | 1610 | 22 | 17 | 43 | 38 | 0.0 |
| | 16x | 305 | 0 | 2 | 188 | −246 | 55 | 1469 | 23 | 12 | 26 | 25 | 0.0 |
| OHU-VarSub | 2x | 294 | −2 | 2 | 93 | −148 | 55 | 1738 | 23 | 47 | 100 | 147 | 0.0 |
| | 4x | 297 | −2 | 1 | 101 | −155 | 55 | 1871 | 24 | 43 | 100 | 136 | 0.0 |
| | 8x | 299 | −2 | 1 | 107 | −161 | 55 | 1971 | 25 | 40 | 100 | 127 | 0.0 |
| | 16x | 303 | −3 | 0 | 125 | −178 | 55 | 2222 | 25 | 35 | 98 | 106 | 0.1 |
| SST-FixSub | 1x | 292 | −2 | 2 | 92 | −147 | 55 | 1688 | 21 | 48 | 100 | 151 | 0.0 |
| | 2x | 295 | −9 | 1 | 108 | −156 | 55 | 1634 | 22 | 43 | 99 | 138 | 0.0 |
| | 4x | 298 | −10 | 1 | 128 | −174 | 55 | 1577 | 23 | 34 | 97 | 115 | 0.0 |
| | 8x | 301 | 26 | 3 | 145 | −229 | 55 | 1337 | 24 | 15 | 48 | 41 | 0.0 |
| | 16x | 304 | 18 | 2 | 170 | −246 | 55 | 1315 | 24 | 11 | 26 | 24 | 0.0 |
| SST-VarSub | 2x | 295 | −3 | 2 | 103 | −156 | 55 | 1870 | 22 | 42 | 100 | 136 | 0.0 |
| | 4x | 298 | −6 | 1 | 114 | −164 | 55 | 2091 | 23 | 38 | 99 | 124 | 0.0 |
| | 8x | 301 | −9 | 1 | 128 | −175 | 55 | 2335 | 23 | 35 | 98 | 108 | 0.1 |
| | 16x | 304 | −35 | 0 | 137 | −157 | 55 | 2725 | 24 | 50 | 99 | 126 | 0.3 |

[a]Data fields as in Table 2.

**Table 4.** Mean Conditions of the S12 Climate Change Experiments During Days 30–40[a]

| EXP | $CO_2$ | SST (K) | IMBAL ($W m^{-2}$) | SHF ($W m^{-2}$) | LHF ($W m^{-2}$) | RAD ($W m^{-2}$) | OHU ($W m^{-2}$) | ZINV (m) | LTS (K) | LWP ($g m^{-2}$) | CC (%) | SWCRE ($W m^{-2}$) | PREC ($mm d^{-1}$) |
|---|---|---|---|---|---|---|---|---|---|---|---|---|---|
| OHU-FixSub | 1x | 290 | 0 | 4 | 84 | −127 | 40 | 830 | 24 | 76 | 100 | 184 | 0.0 |
| | 2x | 293 | −0 | 2 | 102 | −144 | 40 | 830 | 24 | 60 | 98 | 161 | 0.0 |
| | 4x | 302 | 0 | 6 | 193 | −240 | 40 | 991 | 19 | 7 | 17 | 17 | 0.0 |
| | 8x | 304 | 0 | 5 | 201 | −246 | 40 | 901 | 21 | 5 | 16 | 15 | 0.0 |
| | 16x | 306 | −0 | 4 | 209 | −253 | 40 | 820 | 23 | 4 | 15 | 13 | 0.0 |
| OHU-VarSub | 2x | 291 | −1 | 1 | 82 | −122 | 40 | 850 | 26 | 83 | 100 | 187 | 0.0 |
| | 4x | 302 | 4 | 5 | 186 | −235 | 40 | 1388 | 20 | 13 | 27 | 27 | 0.0 |
| | 8x | 304 | 2 | 3 | 195 | −239 | 40 | 1576 | 21 | 14 | 28 | 28 | 0.0 |
| | 16x | 306 | 2 | 1 | 200 | −244 | 40 | 1677 | 23 | 15 | 28 | 28 | 0.0 |
| SST-FixSub | 1x | 290 | −2 | 4 | 84 | −127 | 40 | 830 | 24 | 77 | 100 | 185 | 0.0 |
| | 2x | 293 | 4 | 3 | 98 | −145 | 40 | 810 | 25 | 59 | 98 | 160 | 0.0 |
| | 4x | 296 | 90 | 6 | 86 | −222 | 40 | 527 | 26 | 11 | 58 | 53 | 0.0 |
| | 8x | 299 | 150 | 1 | 62 | −252 | 40 | 510 | 26 | 0 | 0 | 0 | 0.0 |
| | 16x | 302 | 142 | 1 | 76 | −259 | 40 | 510 | 26 | 0 | 0 | 0 | 0.0 |
| SST-VarSub | 2x | 293 | −8 | 0 | 97 | −129 | 40 | 970 | 24 | 74 | 99 | 176 | 0.0 |
| | 4x | 296 | 8 | −0 | 109 | −157 | 40 | 1070 | 25 | 49 | 98 | 140 | 0.0 |
| | 8x | 299 | 97 | 3 | 100 | −241 | 40 | 809 | 26 | 8 | 25 | 24 | 0.0 |
| | 16x | 302 | 76 | 3 | 126 | −244 | 40 | 1016 | 27 | 9 | 31 | 26 | 0.0 |

[a]Data fields as in Table 2.

experiments and results in the SWCRE decrease under warming. However, the inversion height evolves differently between cases: SST-FixSub shows a weak decrease, while SST-VarSub shows a robust increase, as a result of the weakening subsidence. The magnitude of the SWCRE decrease varies widely from 2.3 to

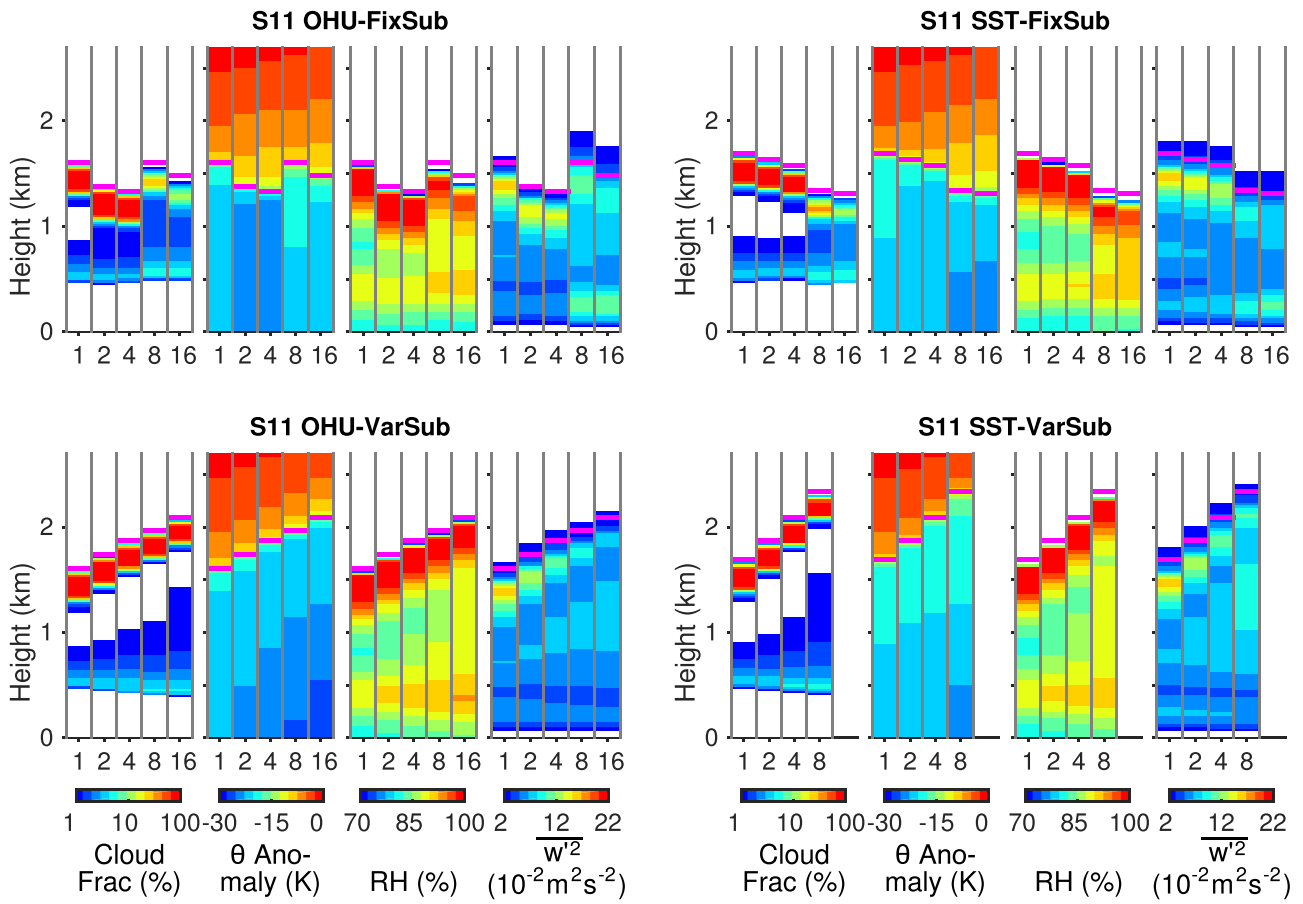


**Figure 6.** Same as Figure 1, but for the S11 climate change experiments during days 30–40.

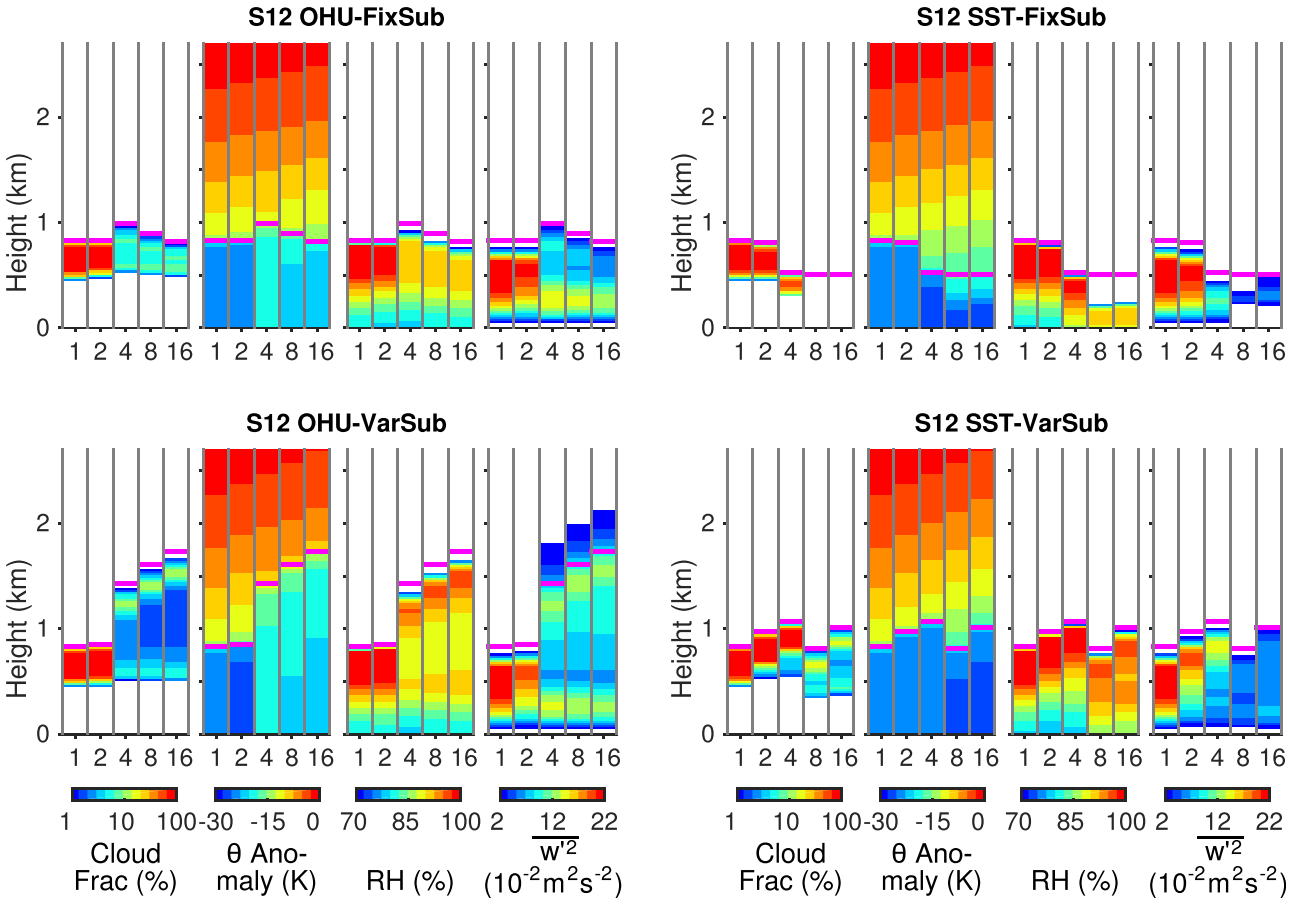


**Figure 7.** Same as Figure 1, but for the S12 climate change experiments during days 30–40.

10.3 W m$^{-2}$ K$^{-1}$. It is stronger with fixed subsidence (SST-FixSub) and for warmer cases, in particular near the transition threshold.

The prescribed-OHU cases show similar trends of MBL characteristics under warming. However, they generally have comparatively lower SST, stronger inversion, and larger LWP than the prescribed-SST cases. The SWCRE decrease is correspondingly weaker, ranging from −1.3 to 6.1 W m$^{-2}$ K$^{-1}$. The negative values correspond to the increased SWCRE for S12 OHU-VarSub and S11 OHU-FixSub cases between 1× and 2×$CO_2$. The SWCRE decrease is also stronger with fixed subsidence (OHU-FixSub) and for warmer cases.

Similar to the S6 cases, an energy budget argument explains the difference between the S11 and S12 cases with prescribed SST and prescribed OHU. With a prescribed SST increase, LHF increases by about 5 % K$^{-1}$ and exceeds the decrease in surface LW radiative cooling. Thus, the surface energy budget is not closed. In contrast, with fixed OHU, LHF is constrained to increase less under warming, which corresponds to lower SST and a stronger inversion. Unlike in the S6 (Cu) cases, the change of SWCRE in the Sc cases is important for the surface energy budget. If the decrease in SWCRE overcompensates the increase in LHF (e.g., S12 OHU-FixSub versus SST-FixSub at 2×$CO_2$), the energetic contrast is reversed, implying that the prescribed-OHU cases are instead warmer and deeper than the prescribed-SST cases. This reversed contrast is most evident during cloud regime transition, when SWCRE decreases by over 100 W m$^{-2}$, as we will discuss next.

### 4.2. Regime Transition From Sc to Cu Under Strong Warming

The cloud regime transition is characterized by the breakup of the Sc layer, during which the cloud cover and LWP both decrease rapidly. This leads to almost complete loss of cloud-top LW cooling and consequently a significant weakening of MBL turbulence, especially just below the inversion.

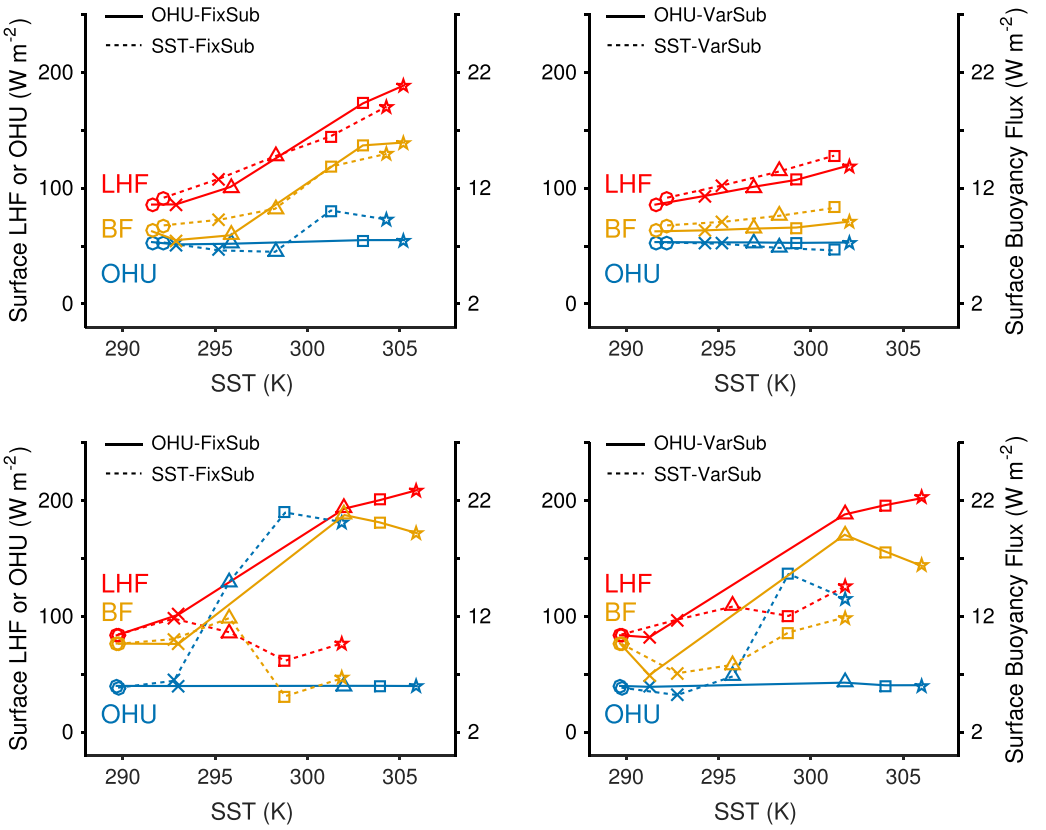


**Figure 8.** Same as Figure 3, but for (top) S11 and (bottom) S12 cases.

With prescribed SST, the MBL-top entrainment rate and inversion height both decrease as MBL turbulence weakens. This is consistent with the MBL energy budget: the decreased LW cooling is compensated by the reduced entrainment heating; the relative reduction in entrainment drying is compensated by the decrease (or reduced increase) in the surface LHF. The steady state is characterized by a shallow Cu layer, or even a clear MBL (S12 SST-FixSub above $8\times CO_2$). The SWCRE decreases by 24–36 $W\,m^{-2}\,K^{-1}$ during the transition, and thus the surface energy budget is not closed, unless OHU can increase as much.

With prescribed OHU, the strong SWCRE feedback during Sc breakup causes the SST to increase by 7 to 11 K, accompanied by a strong decrease in inversion strength. Therefore, the over 100 $W\,m^{-2}$ decrease in SWCRE over the Sc-to-Cu transition converts to only a 13.6–14.6 $W\,m^{-2}\,K^{-1}$ change when normalized by the local SST change. The MBL after the transition becomes much warmer and deeper than in the cases with prescribed SST; it is even deeper than in the Sc regime before the transition. The large increase in surface SW heating is compensated by a comparable increase in LHF, augmented by changes in SHF and LW cooling at the surface. The increased surface buoyancy flux helps maintain the strength of MBL turbulence and MBL-top entrainment, resulting in a relatively deep Cu layer (see Figure 8, orange solid curves).

*Bretherton et al.* [2013] distinguishes four ways in which a Sc layer can respond to warming:

1. Decreased turbulence driving (because of increased free-tropospheric LW opacity and by weaker surface wind) lowers and thins Sc;
2. Reduced large-scale subsidence lifts (and may thicken) Sc;
3. Increased vertical moisture gradient thins Sc; and
4. Increased inversion strength lowers (but may thicken) Sc.

The reduction of LWP and the subsequent breakup of Sc in our warming experiments are mainly related to the first effect, or more specifically, the radiative effects of increased $CO_2$ and water vapor in the free troposphere. The reduced subsidence counteracts the radiative effects in OHU-VarSub and SST-VarSub experiments and delays the Sc breakup until higher $CO_2$ levels are reached. In the experiments with prescribed

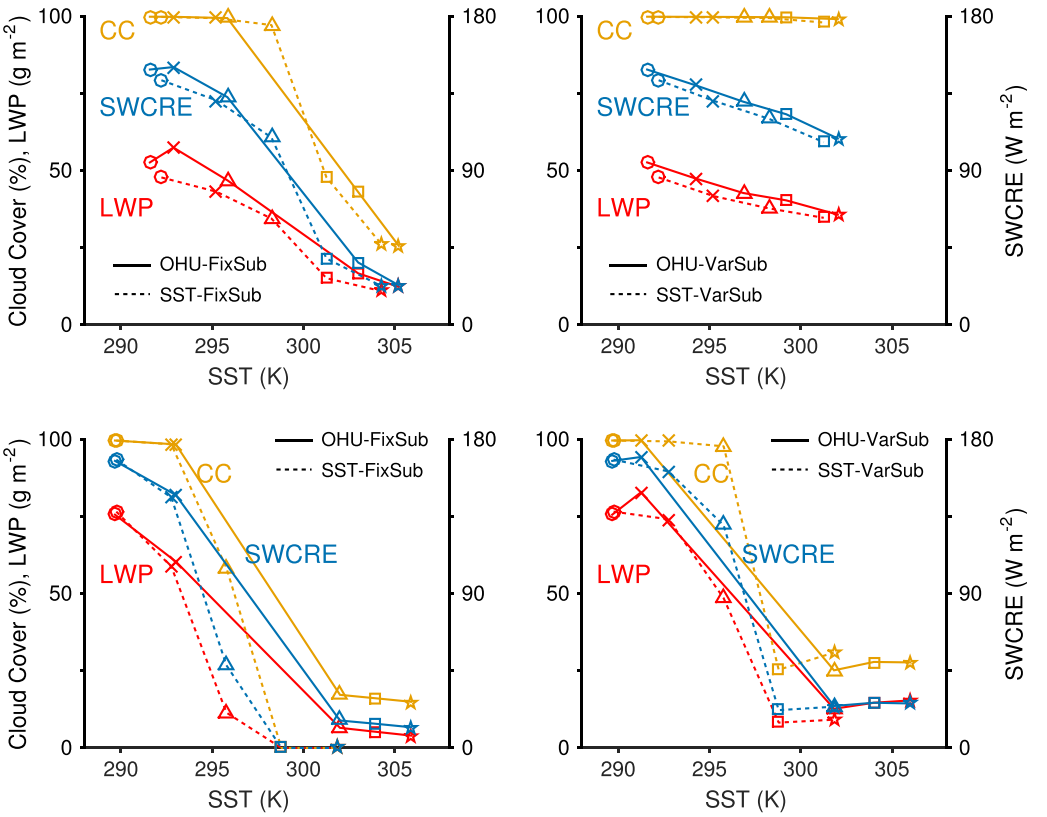


**Figure 9.** Same as Figure 4, but for (top) S11 and (bottom) S12 cases.

OHU, SW cloud feedback affects the SST and influences the Sc layer through the third (moisture gradient) and fourth (inversion strength) effects, both contributing to a more abrupt Sc breakup.

### 4.3. Implication for LTS-SWCRE Relation

Figure 10 shows the average LWP, CC, and SWCRE as functions of LTS during days 30–40. The cases with prescribed SST show a gradual increase of LTS under warming, while the Sc layer gradually thins and eventually breaks up. Therefore, the LTS is negatively correlated with SWCRE, as in the S6 Cu cases.

In contrast, the cases with prescribed OHU show a nonmonotonic LTS trend. The significant SST increase resulting from the Sc breakup causes a 4–6 K abrupt LTS decrease. The decrease of both LTS and SWCRE during Sc breakup appears as a strong positive LTS-SWCRE correlation. However, the LTS-SWCRE correlation is weakly negative both in the Sc regime before the transition and in the Cu regime after the transition. Thus, it remains difficult to use the empirical LTS correlation with CC or SWCRE in the present climate for inferences about changed climates.

### 4.4. Summary

The key results of the Sc (S11 and S12) climate change cases can be summarized as follows:

1. The Sc layer generally breaks up and transitions into a Cu layer when $CO_2$ concentrations increase four to eightfold. The transition threshold is higher for S11 than for S12, and it is higher with reduced subsidence. The Sc breakup is mainly linked to the increased free-tropospheric LW opacity, which weakens the turbulence production by Sc-top cooling.
2. The breakup of the Sc layer leads to an abrupt SWCRE decrease of over 100 $W\,m^{-2}$, which causes an SST increase of 7–10 K in the cases with prescribed OHU. As a result, the MBL after Sc breakup in the cases with prescribed OHU are much warmer and deeper than in the cases with prescribed SST.
3. SWCRE also decreases under modest warming before Sc breakup, but the magnitude varies widely from about 0 to 10 $W\,m^{-2}\,K^{-1}$. The decrease is weaker with prescribed OHU.

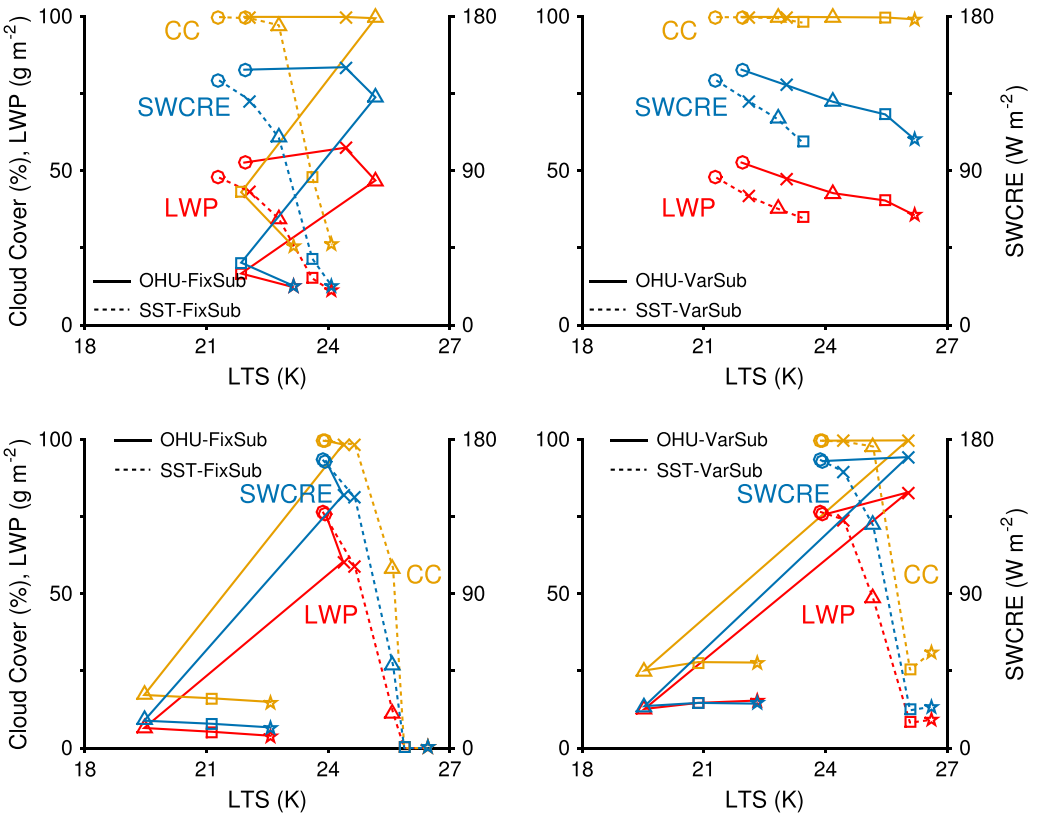


**Figure 10.** Same as Figure 5, but for (top) S11 and (bottom) S12 cases.

4. The LTS-SWCRE correlation is generally negative. However, this correlation is reversed by the abrupt increase of SST (and thus decrease of LTS) during Sc breakup when OHU is fixed.

A breakup of Sc layers like what we see in the LES so far has not been seen in extreme global warming simulations with comprehensive climate models (M. Huber, personal communication, 2016). However, enhanced activity of tropical transient waves associated with atmospheric superrotation has been described to disrupt subtropical low clouds in warm climates, leading to enhanced climate sensitivity at temperatures when the transition to superrotation occurs [*Caballero and Huber*, 2010, 2013]. Our LES results suggest that there is an additional mechanism that can disrupt stratocumulus cover, suggesting climate sensitivity in warm climates may be higher than current climate models suggest.

## 5. Discussion and Conclusion

In this study, we have used the forcing framework of *Tan et al*. [2016] to study the subtropical MBL cloud responses to climate change. This forcing framework is an alternative and extension of the CGILS set-up [*Blossey et al*., 2013]: we have reformulated the large-scale forcing to ensure greater adaptivity across the wide range of climates covered by our study, and we enforce a closed surface energy balance that is necessary to obtain realizable climates, assuming unchanged OHU. These prescribed-OHU simulation results and the underlying mechanisms are contrasted with those of the conventional prescribed-SST experiments.

### 5.1. Cumulus (Cu)

For the Cu (S6) case with fixed large-scale subsidence (FixSub), the prescribed-OHU experiments simulate weaker SST warming in the subtropics than in the deep tropics. Therefore, the inversion strengthens and the MBL shallows, producing larger cloud cover but significantly less LWP. These responses sum up to a modestly positive SW cloud feedback. The prescribed-SST experiments, in which subtropical SST is

prescribed to increase as much as in the tropics, produce a larger increase in surface LHF and a deeper Cu layer with reduced cloud cover, which is consistent with *Rieck et al*. [2012]. These responses sum up to a more robust positive SW cloud feedback. The differences between the prescribed-OHU and prescribed-SST experiments are reduced if the large-scale subsidence is prescribed to decrease under warming (VarSub).

These results highlight the importance of the surface energy balance for the simulated cloud responses to climate change. Especially the sharp contrast between the prescribed-OHU and prescribed-SST experiments with fixed subsidence demonstrates that the inferences about the cloud response to climate change can be much distorted if a closed surface energy balance is not enforced. The reduced contrast in experiments with varying subsidence arises from a fortuitous compensation between subsidence and surface energy balance effects on the MBL dynamics. This compensation cannot be taken for granted.

### 5.2. Stratocumulus (Sc)

For most Sc (S11 and S12) cases, the cloud layer shallows and LWP decreases robustly under warming, apparently because the turbulent mixing driven by cloud top LW cooling is reduced as the free-tropospheric LW opacity increases. Experiments with both prescribed OHU and SST show that Sc breaks up as $CO_2$ increases to 4–8 times its default concentration. Only the Sc-over-Cu case (S11) with reduced subsidence maintains its Sc-layer through 16 times the default $CO_2$ concentration. In prescribed-OHU experiments with a closed surface energy balance, the strong surface SW feedback during Sc breakup causes the SST to increase abruptly by 7–10 K. Therefore, the MBL conditions after Sc breakup are very different between experiments with prescribed OHU and SST.

The threshold for Sc breakup is sensitive to the LES numerics: both S11 and S12 Sc layers break up at about 2 times the default $CO_2$ concentration if the Smargorinsky SGS dissipation is enabled. The SGS dissipation produces too much MBL-top entrainment and causes excessive MBL drying [*Stevens et al*., 2005] (Pressel et al., submitted manuscript, 2016). Increasing the vertical resolution [*Stevens et al*., 2005; *Blossey et al*., 2013] or switching to an anisotropic SGS scheme (e.g., Pressel et al., submitted manuscript, 2016) can remedy this problem and raise the Sc breakup threshold to higher $CO_2$ concentrations.

The slow drift of the S11 OHU experiments toward lower SST indicates that the S11 Sc-over-Cu transitional regime may be unstable to the SST feedback [*Tan et al*., 2016]: a cooling perturbation in SST leads to a shallower and less decoupled Sc layer with higher LWP and stronger SWCRE, which amplifies the SST cooling, and vice versa for a warm perturbation in SST. This leads to bifurcation of cloud regimes into either Sc or Cu steady states. A similar phenomenon was also reported by *Bretherton et al*. [2010], although their destabilizing feedback was provided by the cloud-top LW cooling acting on MBL, since SST was fixed in their study. This implies that the Sc-over-Cu regime might not be in statistical equilibrium, especially if the large-scale synoptic forcing changes faster than the convergence timescale (>40 days in S11 OHU experiments). Including time-varying large-scale forcing in the LES may be important for such situations. The dependence of such transitional cloud regimes on their history also implies that the memory of upstream and past conditions may be important for both LES experiments [*Bretherton and Blossey*, 2014; *Inoue et al*., 2014] and turbulence-convection parameterizations in climate models.

### 5.3. Implications for SW Cloud Feedback and Climate Sensitivity

Our simulations show that subtropical low-cloud SW feedbacks are positive for both Cu and Sc regimes. For the Cu regime, SWCRE decreases by 0.6 to 0.7 $W\,m^{-2}$ per 1 K warming (or by 2% $K^{-1}$ relative to the control climate). This is consistent with comprehensive climate models [*Brient and Schneider*, 2016] and within the range of previous LES studies for Cu [*Bretherton*, 2015]. There remains uncertainty about the exact strength of the SW feedback because of the sensitivity of top-Cu cover to the choice of microphysics scheme. For the Sc regime, the SWCRE decrease is state-dependent and varies between 0 to 10 $W\,m^{-2}$ change per 1 K warming (or by 0 to 6% $K^{-1}$ relative to the control climate). SWCRE strengthens as the climate warms and especially when Sc starts to break up. During the transition from Sc to Cu, the SWCRE decreases by up to 14 $W\,m^{-2}$ per 1 K local warming (or by 8% $K^{-1}$ relative to the control climate). This is accompanied by a local SST increase of 7–10 K. Our simulated Sc SW feedback is stronger than that in CGILS [*Blossey et al*., 2013] and comprehensive climate models, which do not simulate the breakup of Sc. However, our results point in the same direction as those of *Caballero and Huber* [2013], who showed that the climate sensitivity increases in warmer climate states due to an enhanced SW cloud feedback.

In summary, LES have become reliable tools for studying cloud feedbacks, but they have produced a wide variety of results for how clouds respond to warming [*Bretherton*, 2015], and often have produced weaker cloud feedbacks than GCMs [e.g., *Rieck et al*., 2012]. We contend that this large variety of results and some of the discrepancy to GCM simulations stems at least in part from different boundary conditions (e.g., prescribing and fixing SST in LES, versus having closed surface energy budgets in GCMs). Our setup helps ensure that climate changes studied in LES (or in single-column contexts) are closer to being realizable, and closer to being comparable to GCMs. Indeed, the Cu feedbacks we find are consistent with those seen in GCMs. The Sc feedbacks we find are stronger than those seen in GCMs because of Sc breakup. Incorporating various large-scale dynamical factors from GCMs (e.g., the strength of Hadley and Walker circulations, tropical transient wave activity, and midlatitude synoptic wave activity) into the LES may help us understand such discrepancies. Through systematic comparisons between LES and GCM, we can also gain more insights into the coupling mechanisms between subtropical low-cloud SW effects, SST gradients, and the large-scale circulation.

**Acknowledgments**

This work was supported by the U.S. National Science Foundation (grant CCF-1048575), by Caltech's Terrestrial Hazard Observation and Reporting (THOR) Center, and by the Swiss National Science Foundation. The numerical simulations are performed on the Euler Cluster operated by the high performance computing (HPC) team at ETH Zürich. We also thank Chris Bretherton and Peter Blossey for helpful discussions about the experimental design and interpretation of results. The PyCLES code and the configurations for the idealized climate change experiments are available online at climate-dynamics.org/software.

## References

Ackerman, A. S., et al. (2009), Large-eddy simulations of a drizzling, stratocumulus-topped marine boundary layer, *Mon. Weather Rev.*, *137*, 1083–1110, doi:10.1175/2008MWR2582.1.

Balsara, D. S., and C.-W. Shu (2000), Monotonicity preserving weighted essentially non-oscillatory schemes with increasingly high order of accuracy, *J. Comput. Phys.*, *160*, 405–452, doi:10.1006/jcph.2000.6443.

Bellon, G., and B. Stevens (2012), Using the sensitivity of large-eddy simulations to evaluate atmospheric boundary layer models, *J. Atmos. Sci.*, *69*, 1582–1601, doi:10.1175/JAS-D-11-0160.1.

Betts, A. K., and W. Ridgway (1989), Climatic equilibrium of the atmospheric convective boundary layer over a tropical ocean, *J. Atmos. Sci.*, *46*, 2621–2641, doi:10.1175/1520-0469(1989)046 <2621:CEOTAC >2.0.CO;2.

Blossey, P. N., C. S. Bretherton, M. Zhang, A. Cheng, S. Endo, T. Heus, Y. Liu, A. P. Lock, S. R. de Roode, and K.-M. Xu (2013), Marine low cloud sensitivity to an idealized climate change: The CGILS LES intercomparison, *J. Adv. Model. Earth Syst.*, *5*, 234–258, doi:10.1002/jame.20025.

Boer, G. J. (1993), Climate change and the regulation of the surface moisture and energy budgets, *Clim. Dyn.*, *8*, 225–239, doi:10.1007/BF00198617.

Bony, S., and J.-L. Dufresne (2005), Marine boundary layer clouds at the heart of tropical cloud feedback uncertainties in climate models, *Geophys. Res. Lett.*, *32*, L20806, doi:10.1029/2005GL023851.

Bretherton, C. S. (2015), Insights into low-latitude cloud feedbacks from high-resolution models, *Philos. Trans. R. Soc. London A*, *373*, 20140415, doi:10.1098/rsta.2014.0415.

Bretherton, C. S., and P. N. Blossey (2014), Low cloud reduction in a greenhouse-warmed climate: Results from Lagrangian LES of a subtropical marine cloudiness transition, *J. Adv. Model. Earth Syst.*, *6*, 91–114, doi:10.1002/2013MS000250.

Bretherton, C. S., J. Uchida, and P. N. Blossey (2010), Slow manifolds and multiple equilibria in stratocumulus-capped boundary layers, *J. Adv. Model. Earth Syst.*, *2*, 14, doi:10.3894/JAMES.2010.2.14.

Bretherton, C. S., P. N. Blossey, and C. R. Jones (2013), Mechanisms of marine low cloud sensitivity to idealized climate perturbations: A single-LES exploration extending the CGILS cases, *J. Adv. Model. Earth Syst.*, *5*, 316–337, doi:10.1002/jame.20019.

Brient, F., and T. Schneider (2016), Constraints on climate sensitivity from space-based measurements of low-cloud reflection, *J. Clim.*, *29*, 5821–5835, doi:10.1175/JCLI-D-15-0897.1.

Brient, F., T. Schneider, Z. Tan, S. Bony, X. Qu, and A. Hall (2016), Shallowness of tropical low clouds as a predictor of climate models' response to warming, *Clim. Dyn.*, *47*, 433–449, doi:10.1007/s00382-015-2846-0.

Caballero, R., and J. Hanley (2012), Midlatitude eddies, storm-track diffusivity, and poleward moisture transport in warm climates, *J. Atmos. Sci.*, *69*, 3237–3250, doi:10.1175/JAS-D-12-035.1.

Caballero, R., and M. Huber (2010), Spontaneous transition to superrotation in warm climates simulated by cam3, *Geophys. Res. Lett.*, *37*, L11701, doi:10.1029/2010GL043468.

Caballero, R., and M. Huber (2013), State-dependent climate sensitivity in past warm climates and its implications for future climate projections, *Proc. Natl. Acad. Sci. U. S. A.*, *110*, 14,162–14,167, doi:10.1073/pnas.1303365110.

Caballero, R., and P. L. Langen (2005), The dynamic range of poleward energy transport in an atmospheric general circulation model, *Geophys. Res. Lett.*, *32*, L02705, doi:10.1029/2004GL021581.

Caldwell, P., and C. S. Bretherton (2009), Large eddy simulation of the diurnal cycle in Southeast Pacific stratocumulus, *J. Atmos. Sci.*, *66*, 432–449, doi:10.1175/2008JAS2785.1.

Cess, R. D., et al. (1990), Intercomparison and interpretation of climate feedback processes in 19 atmospheric general circulation models, *J. Geophys. Res.*, *95*, 16,601–16,615, doi:10.1029/JD095iD10p16601.

Cess, R. D., et al. (1996), Cloud feedback in atmospheric general circulation models: An update, *J. Geophys. Res.*, *101*, 12,791–12,794, doi:10.1029/96JD00822.

Charney, J. G. (1963), A note on large-scale motions in the tropics, *J. Atmos. Sci.*, *20*, 607–609, doi:10.1175/1520-0469(1963)020 <0607:ANOLSM >2.0.CO;2.

Chung, D., G. Matheou, and J. Teixeira (2012), Steady-state large-eddy simulations to study the stratocumulus to shallow cumulus cloud transition, *J. Atmos. Sci.*, *69*, 3264–3276, doi:10.1175/JAS-D-11-0256.1.

Dufresne, J.-L., and S. Bony (2008), An assessment of the primary sources of spread of global warming estimates from coupled atmosphere–ocean models, *J. Clim.*, *21*, 5135–5144, doi:10.1175/2008JCLI2239.1.

Duynkerke, P. G., P. J. Jonker, A. Chlond, M. C. Van Zanten, J. Cuxart, P. Clark, E. Sanchez, G. Martin, G. Lenderink, and J. Teixeira (1999), Intercomparison of three- and one-dimensional model simulations and aircraft observations of stratocumulus, *Boundary Layer Meteorol.*, *92*, 453–487, doi:10.1023/A:1002006919256.

Forster, P. M., T. Andrews, P. Good, J. M. Gregory, L. S. Jackson, and M. Zelinka (2013), Evaluating adjusted forcing and model spread for historical and future scenarios in the cmip5 generation of climate models, *J. Geophys. Res. Atmos.*, *118*, 1139–1150, doi:10.1002/jgrd.50174.

Gesso, S. D., A. P. Siebesma, S. R. de Roode, and J. M. van Wessem (2014), A mixed-layer model perspective on stratocumulus steady states in a perturbed climate, *Q. J. R. Meteorol. Soc.*, *140*, 2119–2131, doi:10.1002/qj.2282.

Held, I. M., and B. J. Soden (2000), Water vapor feedback and global warming, *Annu. Rev. Energy Environ.*, *25*, 441–475, doi:10.1146/annurev.energy.25.1.441.

Held, I. M., and B. J. Soden (2006), Robust responses of the hydrological cycle to global warming, *J. Clim.*, *19*, 5686–5699, doi:10.1175/JCLI3990.1.

Iacono, M. J., J. S. Delamere, E. J. Mlawer, M. W. Shephard, S. A. Clough, and W. D. Collins (2008), Radiative forcing by long-lived greenhouse gases: Calculations with the AER radiative transfer models, *J. Geophys. Res.*, *113*, D13103, doi:10.1029/2008JD009944.

Inoue, M., G. Matheou, and J. Teixeira (2014), LES of a spatially developing atmospheric boundary layer: Application of a fringe method for the stratocumulus to shallow cumulus cloud transition, *Mon. Weather Rev.*, *142*, 3418–3424, doi:10.1175/MWR-D-13-00400.1.

Jiang, G.-S., and C.-W. Shu (1996), Efficient implementation of weighted ENO schemes, *J. Comput. Phys.*, *126*, 202–228, doi:10.1006/jcph.1996.0130.

Klein, S. A., and D. L. Hartmann (1993), The seasonal cycle of low stratiform clouds, *J. Clim.*, *6*, 1587–1606, doi:10.1175/1520-0442(1993)006<1587:TSCOLS>2.0.CO;2.

Lauer, A., K. Hamilton, Y. Wang, V. T. J. Phillips, and R. Bennartz (2010), The impact of global warming on marine boundary layer clouds over the eastern pacific: A regional model study, *J. Clim.*, *23*, 5844–5863, doi:10.1175/2010JCLI3666.1.

Levine, X. J., and T. Schneider (2011), Response of the Hadley circulation to climate change in an aquaplanet GCM coupled to a simple representation of ocean heat transport, *J. Atmos. Sci.*, *68*, 769–783, doi:10.1175/2010JAS3553.1.

Liu, X.-D., S. Osher, and T. Chan (1994), Weighted essentially non-oscillatory schemes, *J. Comput. Phys.*, *115*, 200–212, doi:10.1006/jcph.1994.1187.

Lu, J., and M. Cai (2009), Stabilization of the atmospheric boundary layer and the muted global hydrological cycle response to global warming, *J. Hydrometeorol.*, *10*, 347–352, doi:10.1175/2008JHM1058.1.

Matheou, G., D. Chung, L. Nuijens, B. Stevens, and J. Teixeira (2011), On the fidelity of large-eddy simulation of shallow precipitating cumulus convection, *Mon. Weather Rev.*, *139*, 2918–2939, doi:10.1175/2011MWR3599.1.

Medeiros, B., and L. Nuijens (2016), Clouds at barbados are representative of clouds across the trade wind regions in observations and climate models, *Proc. Natl. Acad. Sci. U. S. A.*, *113*, E3062–E3070, doi:10.1073/pnas.1521494113.

Mitchell, J. F. B., C. A. Wilson, and W. M. Cunnington (1987), On co2 climate sensitivity and model dependence of results, *Q. J. R. Meteorol. Soc.*, *113*, 293–322, doi:10.1002/qj.49711347517.

O'Gorman, P. A., and T. Schneider (2008a), The hydrological cycle over a wide range of climates simulated with an idealized GCM, *J. Clim.*, *21*, 3815–3832, doi:10.1175/2007JCLI2065.1.

O'Gorman, P. A., and T. Schneider (2008b), Energy of midlatitude transient eddies in idealized simulations of changed climates, *J. Clim.*, *21*, 5797–5806, doi:10.1175/2008JCLI2099.1.

O'Gorman, P. A., and T. Schneider (2009), Scaling of precipitation extremes over a wide range of climates simulated with an idealized GCM, *J. Clim.*, *22*, 5676–5685, doi:10.1175/2009JCLI2701.1.

Peters, M. E., and C. S. Bretherton (2005), A simplified model of the walker circulation with an interactive ocean mixed layer and cloud-radiative feedbacks, *J. Clim.*, *18*, 4216–4234.

Pierrehumbert, R. T. (1995), Thermostats, radiator fins, and the local runaway greenhouse, *J. Atmos. Sci.*, *52*, 1784–1806, doi:10.1175/1520-0469(1995)052<1784:TRFATL>2.0.CO;2.

Pierrehumbert, R. T. (2002), The hydrologic cycle in deep-time climate problems, *Nature*, *419*, 191–198.

Pressel, K. G., C. M. Kaul, T. Schneider, Z. Tan, and S. Mishra (2015), Large-eddy simulation in an anelastic framework with closed water and entropy balances, *J. Adv. Model. Earth Syst.*, *7*, 1425–1456, doi:10.1002/2015MS000496.

Rieck, M., L. Nuijens, and B. Stevens (2012), Marine boundary layer cloud feedbacks in a constant relative humidity atmosphere, *J. Atmos. Sci.*, *69*, 2538–2550, doi:10.1175/JAS-D-11-0203.1.

Schalkwijk, J., H. J. J. Jonker, and A. P. Siebesma (2013), Simple solutions to steady-state cumulus regimes in the convective boundary layer, *J. Atmos. Sci.*, *70*, 3656–3672, doi:10.1175/JAS-D-12-0312.1.

Schneider, T. (2007), The thermal stratification of the extratropical troposphere, in *The Global Circulation of the Atmosphere*, edited by T. Schneider and A. H. Sobel, pp. 47–77, Princeton Univ. Press, Princeton, N. J.

Schneider, T., and C. C. Walker (2006), Self-organization of atmospheric macroturbulence into critical states of weak nonlinear eddy-eddy interactions, *J. Atmos. Sci.*, *63*(6), 1569–1586, doi:10.1175/JAS3699.1.

Schneider, T., P. A. O'Gorman, and X. J. Levine (2010), Water vapor and the dynamics of climate changes, *Rev. Geophys.*, *48*, RG3001, doi:10.1029/2009RG000302.

Seifert, A., and K. D. Beheng (2001), A double-moment parameterization for simulating autoconversion, accretion and self-collection, *Atmos. Res.*, *59–60*, 265–281, doi:10.1016/S0169-8095(01)00126-0.

Seifert, A., and K. D. Beheng (2006), A two-moment cloud microphysics parameterization for mixed-phase clouds. Part 1: Model description, *Meteorol. Atmos. Phys.*, *92*, 45–66, doi:10.1007/s00703-005-0112-4.

Siebesma, A. P., et al. (2003), A large eddy simulation intercomparison study of shallow cumulus convection, *J. Atmos. Sci.*, *60*, 1201–1219, doi:10.1175/1520-0469(2003)60<1201:ALESIS>2.0.CO;2.

Singh, M. S., and P. A. O'Gorman (2013), Influence of entrainment on the thermal stratification in simulations of radiative-convective equilibrium, *Geophys. Res. Lett.*, *40*, 4398–4403, doi:10.1002/grl.50796.

Singh, M. S., and P. A. O'Gorman (2015), Increases in moist-convective updraught velocities with warming in radiative-convective equilibrium, *Q. J. R. Meteorol. Soc.*, *141*, 2828–2838, doi:10.1002/qj.2567.

Sobel, A. H., and C. S. Bretherton (2000), Modeling tropical precipitation in a single column, *J. Clim.*, *13*, 4378–4392, doi:10.1175/1520-0442(2000)013<4378:MTPIAS>2.0.CO;2.

Sobel, A. H., J. Nilsson, and L. M. Polvani (2001), The weak temperature gradient approximation and balanced tropical moisture waves, *J. Atmos. Sci.*, *58*, 3650–3665, doi:10.1175/1520-0469(2001)058<3650:TWTGAA>2.0.CO;2.

Stevens, B., and A. Seifert (2008), Understanding macrophysical outcomes of microphysical choices in simulations of shallow cumulus convection, *J. Meteorol. Soc. Jpn.*, *86A*, 143–162, doi:10.2151/jmsj.86A.143.

Stevens, B., et al. (2005), Evaluation of large-eddy simulations via observations of nocturnal marine stratocumulus, *Mon. Weather Rev.*, *133*, 1443–1462, doi:10.1175/MWR2930.1.

Tan, Z., T. Schneider, J. Teixeira, and K. G. Pressel (2016), Large-eddy simulation of subtropical cloud-topped boundary layers: 1. A forcing framework with closed surface energy balance, *J. Adv. Model. Earth Syst.*, *8*, 1565–1585, doi:10.1002/2016MS000655.

Teixeira, J., et al. (2011), Tropical and subtropical cloud transitions in weather and climate prediction models: The GCSS/WGNE Pacific cross-section intercomparison (GPCI), *J. Clim.*, *24*, 5223–5256, doi:10.1175/2011JCLI3672.1.

van der Dussen, J. J., S. R. de Roode, S. D. Gesso, and A. P. Siebesma (2015), An les model study of the influence of the free tropospheric thermodynamic conditions on the stratocumulus response to a climate perturbation, *J. Adv. Model. Earth Syst.*, *7*, 670–691, doi:10.1002/2014MS000380.

van Zanten, M. C., et al. (2011), Controls on precipitation and cloudiness in simulations of trade-wind cumulus as observed during RICO, *J. Adv. Model. Earth Syst.*, *3*, M06001, doi:10.1029/2011MS000056.

Vial, J., J.-L. Dufresne, and S. Bony (2013), On the interpretation of inter-model spread in CMIP5 climate sensitivity estimates, *Clim. Dyn.*, *41*, 3339–3362, doi:10.1007/s00382-013-1725-9.

Walker, C. C., and T. Schneider (2006), Eddy influences on Hadley circulations: Simulations with an idealized GCM, *J. Atmos. Sci.*, *63*, 3333–3350, doi:10.1175/JAS3821.1.

Webb, M. J., and A. P. Lock (2013), Coupling between subtropical cloud feedback and the local hydrological cycle in a climate model, *Clim. Dyn.*, *41*, 1923–1939, doi:10.1007/s00382-012-1608-5.

Webb, M. J., et al. (2006), On the contribution of local feedback mechanisms to the range of climate sensitivity in two GCM ensembles, *Clim. Dyn.*, *27*, 17–38, doi:10.1007/s00382-006-0111-2.

Wood, R., and C. S. Bretherton (2006), On the relationship between stratiform low cloud cover and lower-tropospheric stability, *J. Clim.*, *19*, 6425–6432.

Xu, K.-M., A. Cheng, and M. Zhang (2010), Cloud-resolving simulation of low-cloud feedback to an increase in sea surface temperature, *J. Atmos. Sci.*, *67*, 730–748, doi:10.1175/2009JAS3239.1.

Zhang, M., C. S. Bretherton, P. N. Blossey, S. Bony, F. Brient, and J.-C. Golaz (2012), The CGILS experimental design to investigate low cloud feedbacks in general circulation models by using single-column and large-eddy simulation models, *J. Adv. Model. Earth Syst.*, *4*, M12001, doi:10.1029/2012MS000182.

Zhao, M., J. C. Golaz, I. M. Held, V. Ramaswamy, S. J. Lin, Y. Ming, P. Ginoux, B. Wyman, L. J. Donner, D. Paynter, and H. Guo (2016), Uncertainty in model climate sensitivity traced to representations of cumulus precipitation microphysics, *J. Clim.*, *29*, 543–560, doi:10.1175/JCLI-D-15-0191.1.